CONSTRUCTING SOLAR ENERGY STORAGE MATERIAL USING TiO_2-WO_3 NANOCOMPOSITE AND ITS APPLICATION TO CHROMIUM REDUCTION IN WATER

A Thesis

by

RAND ESSAM FAYEZ YOUSF ELSHORAFA

Submitted to the Office of Graduate and Professional Studies of
Texas A&M University
in partial fulfillment of the requirements for the degree of

MASTER OF SCIENCE

Chair of Committee,	Ahmed Abdel-Wahab
Committee Members,	Mohamed Nounou
	Ibrahim Hassan
Head of Department,	Nazmul Karim

August 2016

Major Subject: Chemical Engineering

ABSTRACT

Metal oxide (TiO_2 and WO_3) heterojunction material was developed in order to harvest light, store solar energy, and apply them to water treatment. Two TiO_2 structures were applied, i.e., TiO_2 nanoparticles (TiNP) and TiO_2 nanotube (TiNT); and were hybridized with WO_3 using different weight ratios of TiO_2 to WO_3 (e.g., 25:75, 50:50, 75:25). To investigate the ability of the TiO_2-WO_3 composite to utilize the captured electrons, hexavalent chromium (Cr(VI)) was used as model target compound. Three different treatment systems were investigated: a) batch photocatalytic system using dispersed particles, b) photoelectrochemical (PEC) system, and c) composites-laden membrane filtration system. The batch system showed that using TiNP resulted in complete Cr(VI) reduction at acidic and neutral pH, whereas TiNT were less effective even at low pH. The surface properties of TiNP and TiNT were characterized to investigate the effect of TiO_2 morphology on their photocatalytic activities. TiNP was found to have a greater photocatalytic activity than TiNT because it is more crystalline, has less structural oxygen defects, has slower recombination of the photogenerated electrons, and has more oxygen vacancies closer to the conduction band (CB). These results were the basis for designing the composites of TiNP- WO_3 and TiNT-WO_3 and characterizing their performances.

In the PEC system where different combinations and weight ratios of TiNP or TiNT to WO_3 were evaluated, TW25 showed the best performance among all combinations. It was able to completely reduce Cr(VI) to Cr(III) in 4 hours of reaction

time under light irradiation as well as in the dark. However, only 70 % of initial Cr(VI) concentration was reduced in 4 hours of reaction time with TNW 25 under the same experimental conditions. The surface properties of the TW and TNW electrodes were characterized using SEM/EDS, elemental mapping, and UV-Vis spectra in order to investigate surface morphology, elemental composition, and flat-band position of the composites.

The composites-laden membrane filtration system using charged TiO_2-WO_3 composite materials showed the feasibility of reducing Cr(VI) to Cr(III) at natural pH. Cr(VI) reduction was more substantial in the system using TW 50 than in the system where material TNW 50 was utilized.

DEDICATION

This thesis is dedicated to my parents for their unconditional love.

ACKNOWLEDGEMENTS

I would like to thank my committee chair Dr. Ahmed Abdel-Wahab and my committee members, Dr. Mohamed Nounou and Dr.Ibrahim Hassan for their support through the research.

I would like to thank Dr. Dong Suk Han who monitored my lab work through the research. I would also like to thank my colleagues, faculties, and staff at Texas A&M University at Qatar.

Special thanks to my father, mother, and siblings for the love and support they provided to me during my graduate study.

NOMENCLATURE

MCL	Maximum Contaminant Level
MCLG	Maximum Contaminant Level Goal
DL	Detection Limit
TiNT	Titanium Dioxide Nanotubes
TiNP	Titanium Dioxide Nanoparticles
TW	Titanium Dioxide Nanoparticles and Tungsten Trioxide
TNW	Titanium Dioxide Nanotubes and Tungsten Trioxide
CB	Conduction Band
VB	Valence Band
PEG	Polyethylene Glycol
FTO	Fluorine Doped Tin Oxide
C	Concentration
C0	Initial Concentration
Ppm	Parts Per Million
T	Time
Min	Minutes
Hr	Hours
Cr(VI)	Hexavalent Chromium

Cr(III)	Trivalent Chromium
XPS	X-Ray Photoelectron Spectroscopy
XRD	X-Ray Diffraction
SEM	Scanning Electron Microscopy
TEM	Transmission Electron Microscopy
EDS	Energy-Dispersive X-Ray Spectroscopy
PL	Photoluminescence Spectra
EtOH	Ethanol
MV^{2+}	Methyl Viologen

TABLE OF CONTENTS

Page

LIST OF FIGURES

Page

Page

LIST OF TABLES

1 INTRODUCTION

The global demand on drinking water is increasing continuously due to population growth and socioeconomic development.[1] In 2006, it was reported by the United Nations that seven hundred million people globally live in water-stressed countries. By 2025, this number will increase by about three billion.[2] Maximizing water reuse and recycle will alleviate stress on fresh water resources and will minimize environmental impact of contaminants release to the environment. This requires sustainable and cost-effective treatment methods for contaminated water and wastewater to meet quality requirements for reuse/recycle or safe disposal. Many treatment technologies transform the contaminant from one phase to another or concentrate it without destroying it or converting to more environmentally benign forms. However, oxidation-reduction treatment methods have the potential of destroying environmental contaminants or converting them to less harmful compounds. Photocatalytic oxidation and reduction using metal semiconductors is an emerging technology for contaminated water treatment.

The purpose of this study is to design and manufacture photocatalysts and develop them into effective treatment systems for Cr(VI) reduction to the less toxic and less mobile Cr(III) under sun light as well as in the light-limited condition. To do so, two experimental approaches were suggested and evaluated in this study: batch treatment system, continuous flow system using photoelectrochemical (PEC) process, or ultrafiltration (UF) membrane system. In the batch treatment system, nanoparticles and nanotubes of TiO_2

(TiNP, TiNT) were used, and TiO_2/WO_3-doposited membrane system was devised for the continuous treatment system.

Effectiveness of batch-scale photocatalytic reduction of Cr(VI) was evaluated in terms of kinetic decay of Cr(VI) using TiNP and TiNT without WO_3. The effect of TiO_2 type on the rate and extent of photocatalytic reduction of Cr(VI) was evaluated by these batch experiments. Eventually, results of these experiments provided information that was used to describe the performance of the TiO_2/WO_3 heterojunction in the PEC and UF systems. For the batch system, formic acid (FA) was used as a photogenerated hole scavenger at the valence band (VB) of TiO_2 for more facile photocatalytic reduction of Cr(VI) on its conduction band (CB).

The PEC system was designed to continuously reduce Cr(VI) to Cr(III) in light-limited condition with WO_3 in the TiO_2-WO_3 composite capable of storing solar energy through charging/discharging route. Herein, different weight ratios of TiO_2/WO_3 were applied for evaluation of Cr(VI) reduction while investigating photocurrent density of charged TiO_2/WO_3 before and after treating water contaminated with Cr(VI).

The UF system using TiO_2/WO_3-laden membrane was constructed to reduce Cr(VI) to Cr(III) in continuous flow system in the dark. To do so, the charged TiO_2/WO_3 composites were deposited on anodic membrane filter (20 nm of pore size). This system combines the advantages of photocatalytic reduction of Cr(VI) and immobilization of the photocatalyst on the filter surface without the need for additional step to recover the photocatalyst after treatment.

2 BACKGROUND

2.1 Photocatalysis

Semiconductors (SC), such as TiO_2, WO_3, ZnO, SnO_2, ZrO_2, $KTaO_3$, $SrTiO_3$, ZnS, and SiC are used as photocatalysts that can be activated by absorbing photon energy higher than the band gap energy of the SC.[3] Figure 1 illustrates the band gab energy and band edge positions of some SC with respect to water oxidation and reduction. Once the SC is activated, the electron-hole pairs are generated by transfer of electrons (e^-) from the valance band (VB) to the conduction band (CB). This photogenerated electron-hole pairs can create reactive chemical species from O_2 and H_2O as shown in reactions (2.1-2.3) when TiO_2 is used as a photocatalyst.[4] The adsorbed chemicals in reaction 2.2 and 2.3 are referred as ads.

$$TiO_2 + hv = TiO_2 + e_{CB}^- + h_{VB}^+ \quad (2.1)$$

$$TiO_{2(substrate)} - H_2O + h_{VB}^+ = TiO_{2(substrate)} - OH_{(ads)} \quad (2.2)$$

$$O_{2(ads)} + e_{CB}^- = O_{2(ads)}^- \quad (2.3)$$

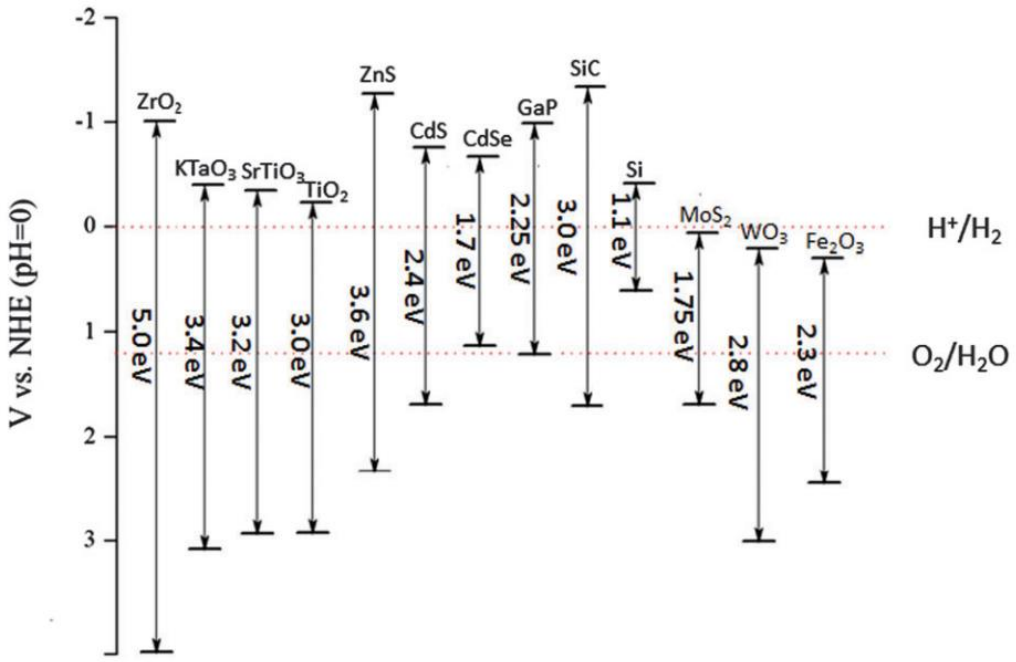

Figure 1. Diagram of band gaps and band edges (CB bottom and VB top) at room temperature [5]

However, a major challenge utilizing the photogenerated electron-hole pairs effectively in redox reactions is the fast recombination of the photogenerated electrons and holes within milli-seconds.[6] Therefore, organic chemicals such as ethanol, humic acid, and formic acid are usually used as a hole scavenger to free the electrons in the conduction band of the SC and allow them to reduce target oxidized contaminants.[7] Another way to overcome the recombination problem is to form heterojunctions with another SC that has higher CB or lower CB. For example, Cu_2O and WO_3 have higher and lower conduction bands respectively compared to TiO_2.[8-10] When they were combined to TiO_2, they showed a success in improving photocatalysis efficiency.

2.1.1 Titanium dioxide semiconductor

TiO_2 has been widely used in the past decades as a photocatalyst in various applications due to its low cost and nontoxicity as well as its appropriate band position with respect to the potential of water oxidation and reduction (Figure 1 and Figure 2). In this regard, TiO_2 can easily produce reactive oxygen species (ROS) such as hydroxide radical ($OH^{\cdot}$), and superoxide (O_2^{-}) by the photogenerated positive holes in the presence of oxygen. The ROS can oxidize organics and degrade them into their constituent elements.[11] Whereas, the photogenerated electron of TiO_2 can reduce toxic inorganic chemicals such as Cr(VI), Se(IV), and Hg(II) to less toxic forms of Cr(III), Se(0), and Hg(0), respectively when a hole scavenger is present in the solution.[12-14] Moreover, co-catalysts RuO or IrO can be added to TiO_2 system to enhance the transfer of the charge carriers.[15]

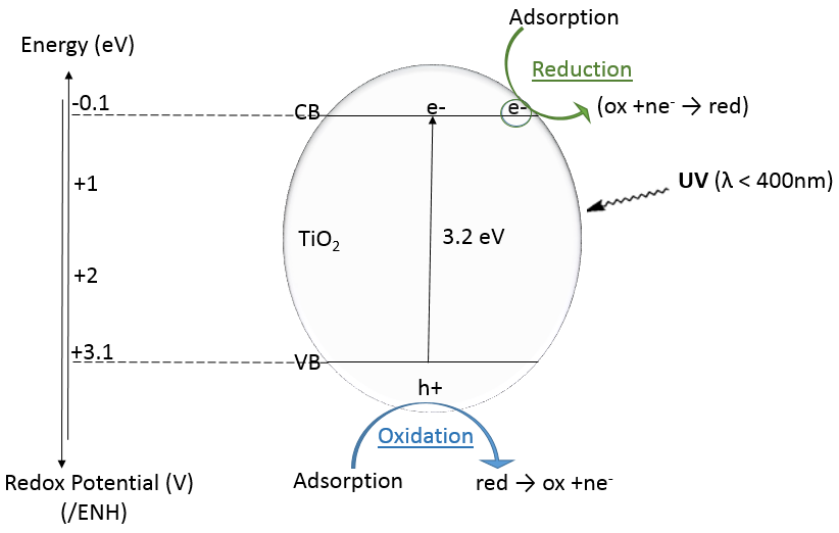

Figure 2. Energy band diagram of anatase titania.[3]

2.1.2 WO_3/TiO_2 system

Tungsten trioxide (WO_3) have a bandgab energy of 2.8 eV and absorption wavelength (λ) of 443 nm.[16] When it is combined with TiO_2, the photocatalytic activity is enhanced because the photogenerated electrons of the TiO_2 particle moves to the CB of WO_3, resulting in retarding the recombination of the charge carriers. This is possible because the band edge position of WO_3 is relatively lower than that of TiO_2 and WO_3 has a lower bandgab energy than TiO_2 (3.2eV, λ=388 nm). [16] Recently, TiO_2/WO_3 composite have been widely studied because of facile movement of photogenerated electrons from TiO_2 to the conduction band of WO_3 during irradiation time. WO_3 has the ability to store electrons during irradiation and discharge them to electron acceptors in the absence of irradiation.[17,18] Thus, TiO_2 is a light-harvesting material, while WO_3 is a light storing material. The following equations show the electron charging and discharging process of TiO_2/WO_3 system:[19]

$$e_{cb}^{-}(TiO_2) \rightarrow e_{cb}^{-}(WO_3)(interfacial\ electron\ transfer) \quad (2.4)$$

$$WO_3 + xe_{cb}^{-} + xH^{+} \rightarrow H_xW^{(6-x)}O_3(photocharging) \quad (2.5)$$

$$H_xW^{(6-x)}O_3 \rightarrow WO_3 + xe_{cb}^{-} + xH^{+}(discharging) \quad (2.6)$$

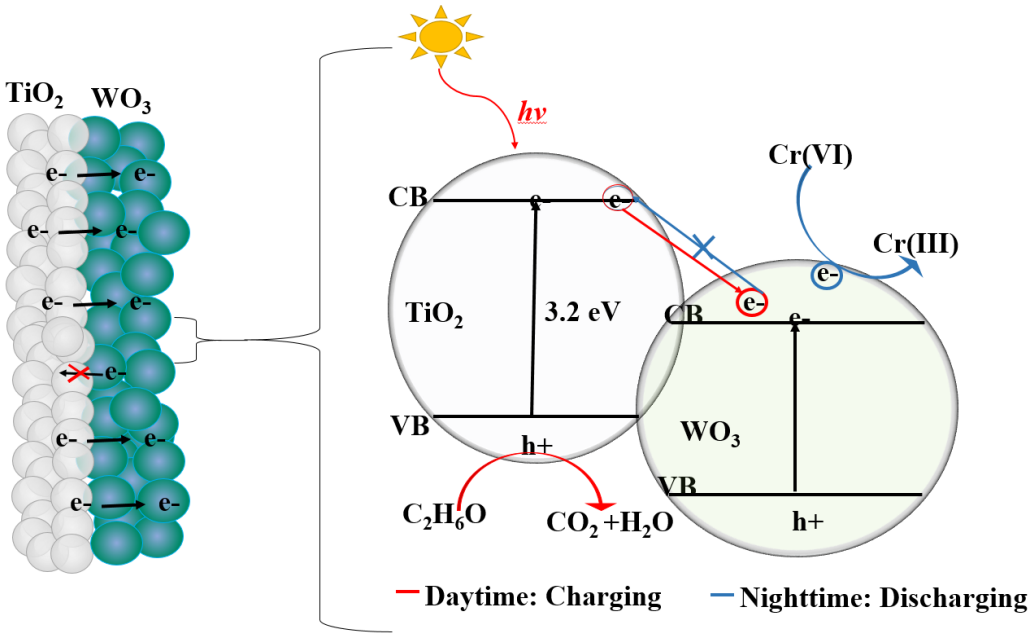

Figure 3. Schematic diagram of charging and discharging process of TiO_2/WO_3 composite system

Other SCs such as Cu_2O, polyoxometalates, and MoO_3 showed their ability to store photo energy. However, WO_3 demonstrated a better performance in storing the photo-generated electrons for around 12 hours.[18] This is attributed to the CB level of WO_3 that is more positive compared to hydrogen reduction potential which results in avoiding competitive consumption of the stored electrons.[18]

In this study, the WO_3/TiO_2 system was investigated to enhance photocatalytic reduction of Cr(VI) in the absence of light by employing two different systems, *i.e.*, photoelectrochemical (PEC) system using photocathode and photocatalytic ultrafiltration (UF) system. Herein, two types of TiO_2 structures were used for fabrication of TiO_2-WO_3 composite (nanoparticle and nanotube) which were deposited on Fluorine doped Tin

Oxide (FTO) glass in the PEC system and were laden onto the surface of the membrane in the UF system. The two systems were evaluated for continuous reduction of Cr(VI) in water.

2.2 Chromium

2.2.1 Chromium chemistry

Chromium is a transition metal element that exists in several oxidation states such as Cr(VI), Cr(V), Cr(IV), Cr(III), Cr(II), Cr(I) and the elemental form Cr(0).[20] Among these forms, hexavalent chromium and trivalent chromium are the most stable forms that are commonly found in nature.[21] According to the United States Environmental Protection Agency (US EPA), Cr(III) is an essential element in the human body and can be added to vitamins as a dietary supplement.[22] The hexavalent form of chromium (Cr(VI)) is 10 ~ 100 times more toxic and it is more mobile than the trivalent form (Cr(III)). Hence, Cr(VI) is categorized as a toxic chemical, while the trivalent form is much less toxic.[23] The oxidation potential values of Cr(VI) and Cr(III) are +1.33 and -0.74 V, respectively. Table 1 represents the half reduction equations for Cr(VI) and Cr(III). Cr(VI) can be reduced in human body to its intermediate product Cr(V) and subsequently to its final product Cr(III) and some free radicals such as $OH\cdot$, O, O_2^-, $RS\cdot$, or $R\cdot$ are formed which can bind the DNA where $RS\cdot$ refers to a thiyl radical (sulfur containing radical) and $R\cdot$ refers to a hydrocarbon radical.[24] This series of reductions damage the DNA by the cross-links forms in the DNA-proteins it.[25] The maximum contaminant level (MCL) of total chromium set

by USEPA is 100 µg/L (ppb) and The maximum contaminant level goal (MCLG) is set to 100 µg/L.[26]

Table 1. Comparison between the reduction potential of Cr(VI) and Cr(III)[27]

Reduction Half reaction	Potential (V)	
$Cr^{3+}_{(aq)} + 3e^- \Longrightarrow Cr(s)$	-0.74	(2.7)
$Cr_2O_7^{2-}{}_{(aq)} + 14\ H^+ + 6e^- \Longrightarrow 2\ Cr^{3+}{}_{(aq)} + 7\ H_2O$	+1.33	(2.8)

Cr(VI) is released to the environment from industrial activities such as electroplating, metal finishing, and textile/leather dyeing. In 1997, 3391 facilities produced 111384 pounds of chromium waste.[20] Improper disposal of soil or residuals contaminated with chromium to landfills can lead to groundwater contamination.[20] If Cr(VI) is released to aquatic environment, Cr (VI) can exist in four different forms depending on its concentration and the pH of the solution as shown in Figure 4. These forms are very soluble in water and do not precipitate easily due to their high solubility products (K_{sp}), while the Ksp value for $Cr(OH)_3$ is very low as shown in Table 2.

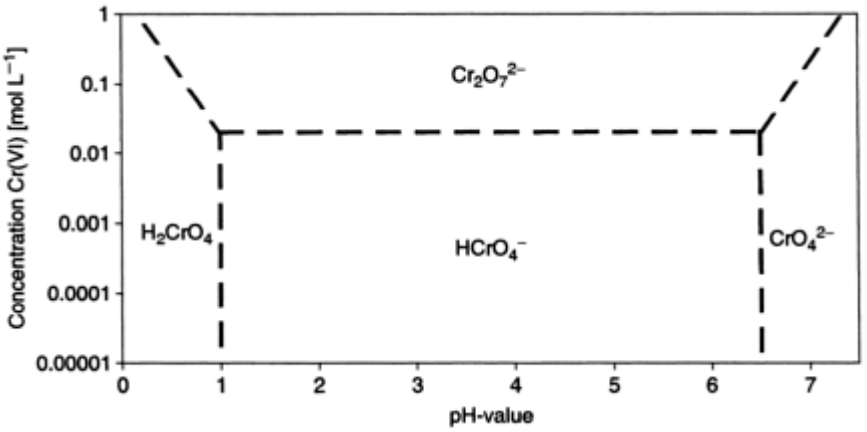

Figure 4. pH and concentration-dependent domains of Cr(VI)-species in aqueous solution[28]

Table 2. Solubility constant of chromium species[29]

Reaction	K_{sp}	
$Cr(OH)_3$ (s) <===> $Cr^{+3} + 3OH^-$	10^{-30} M^{-4}	(2.9)
K_2CrO_4 <===> $CrO_4^{-2} + 2K^+$	0.23 M^3	(2.10)
Na_2CrO_4 <===> $CrO_4^{-2} + 2Na^+$	3.65 M^3	(2.11)
$K_2Cr_2O_7$ <===> $Cr_2O_7^{-2} + 2K^+$	4.9×10^{-3} M^3	(2.12)
$Na_2Cr_2O_7$ <===> $Cr_2O_7^{-2} + 2Na^+$	5.1×10^2 M^3	(2.13)

*M=mole/L

2.2.2 Current methods for Cr(VI) reduction in water

Several treatment technologies have been utilized to reduce Cr(VI) to Cr(III) which include chemical or electrochemical treatment, microbial remediation, photocatalytic treatment, and others. Reducing reagents such as sulfur compounds and iron salts have been used for chemical reduction of Cr(VI). Sulfur dioxide gas or sodium

bisulfite produces sulfurous acid that reduces Cr(VI) in acidic media.[30] This reaction is followed by increasing pH using a base such as sodium hydroxide to precipitate Cr(III) as $Cr(OH)_3$. The following reaction describes the reduction of Cr(VI) by sulfurous acid.

$$Cr^{3+} + H_2SO_{3\ (aq)} + H^{+}_{\ (aq)} \rightarrow Cr^{3+} + SO_3^{2-} + \frac{3}{2}H_2 \qquad (2.14)$$

The most commonly used iron compounds for the chemical reduction of Cr(VI) are iron(II) chloride or iron(II) sulfate.[31] The following reaction describes the reduction of Cr(VI) by Fe(II) in acidic media followed by precipitation reaction at alkaline conditions.

$$6Fe^{2+}_{(aq)} + Cr_2O_7^{2-}{}_{(aq)} + 14H^{+}_{(aq)} \rightarrow 6Fe^{3+}_{(aq)} + 2Cr^{3+}_{(aq)} + 7H_2O \qquad (2.15)$$

$$Cr(III)^{3+}_{(aq)} + 3OH^{-}_{(aq)} \rightarrow Cr(OH)_{3\,(s)} \qquad (2.16)$$

Regardless of the type of chemical reagents used for reduction of Cr(VI), chemical treatment requires excessive amounts of chemicals in order to first reduce the pH to facilitate reduction of Cr(VI) and then raise the pH up to the level required for precipitation of the reduced Cr(III) in addition to the reducing reagents.

Electrochemical treatment of Cr(VI) has attracted attention because this process uses aqueous electron as an environmental-friendly active reagent.[32] The electrochemical processes include electro-reduction and electrocoagulation. The electrocoagulation process is comprised of anode and cathode. Sacrificial electrodes of iron or aluminum metals are mostly used as the anodes for reduction of Cr(VI).[33] In the system with iron electrodes, the anode is oxidized by applying voltage and producing ferrous iron (Fe^{2+})

which reduces the hexavalent chromium ions. This reaction is initiated first at low pH for oxidative release of Fe(II) from the zero-valent Fe electrode and reduction of Cr(VI) by Fe(II). Then the pH is adjusted to high pH for precipitating the reduced Cr(III). Hydrogen gas is released at the cathode surface which enhances floatation of precipitates to the surface as shown in Figure 5. The cathodic and anodic reactions when iron is used as an anode are presented in Table 3. Besides, carbon-based electrodes, conducting polymer-based electrodes, and copper electrodes have been used to electrochemically reduce Cr(VI). [34-36]

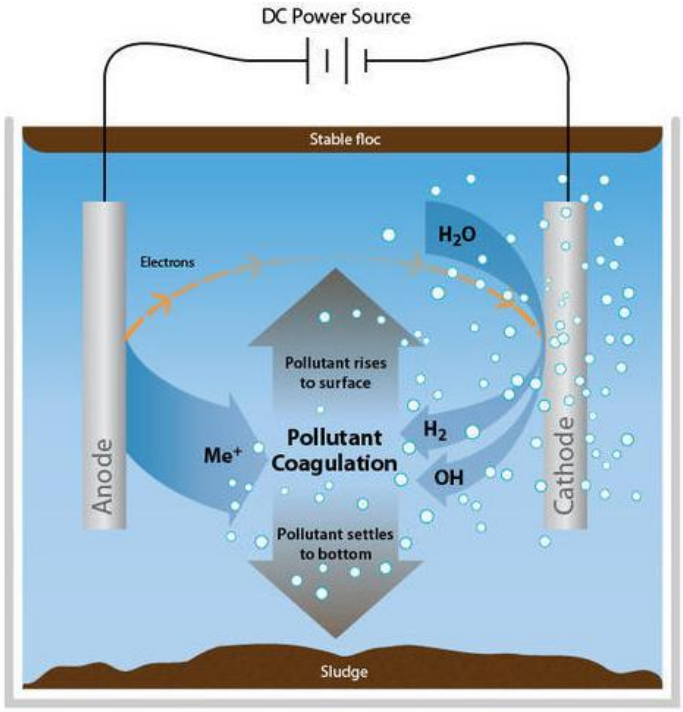

Figure 5. Schematic diagram of electrocoagulation treatment process[35]

Table 3. Anodic and cathodic reactions in electrocoagulation process of Cr(VI) removal[30]

Type of reaction	Reaction	
Anodic reaction	$Fe_{(s)} \rightarrow Fe^{2+}_{(aq)} + 2e^-$	(2.17)
Cathodic reation	$2H_2O + 2e^- \rightarrow 2OH^-_{(aq)}+)$	(2.18)
Overall reaction in bulk	$Cr_2O_7^{2-}{}_{(aq)} + 14H^+_{(aq)} + 6Fe^{2+}_{aq)} \rightarrow$ $2Cr^{3+}_{(aq)} + 6Fe^{3+}_{(aq)} + 7H_2O$	(2.19)
	$Cr^{3+}_{(aq)} + 3OH^-_{aq} \rightarrow Cr(OH)^-_{(s)}$	(2.20)

For the microbial removal of Cr(VI), aerobic reducing bacteria such as *Bacillus Subtillis* and anaerobic reducing bacteria such as *Pannonibacter phragmitetus* were investigated.[37,38] Also, fungi such as *Aspergillus sp. N2* and *Penicillium sp. N3* can also reduce Cr(VI) to Cr(III).[39] However, the disadvantage of using microbes in water treatment process is that it introduces a microbial waste to the system that requires further treatment.

2.2.3 Photocatalytic reduction of hexavalent chromium

Photocatalytic reduction of Cr(VI) has been investigated using TiO_2 with organic acids such as formic acid, acetic acid, methanol, ethanol, or triethanolamine as electron donor or hole scavenger. [40-42] Under light illumination, the organic acid is oxidized by photo-generated positive holes in the VB producing water and CO_2, while the photo-generated electrons in the CB are used to reduce Cr(VI) as shown in Figure 6. Different homogeneous and heterogeneous TiO_2 materials with various structures and compositions

have been evaluated for Cr(VI) reduction. For example TiO_2 nanofibers fabricated by high temperature calcination have been tested for simultaneous phenol degradation and Cr(VI) reduction.[43] Also, heterogeneous TiO_2 such as $La_2TiO_2O_7$ was able to reduce Cr(VI) at acidic pH (pH~2) under UV light irradiation.[44]

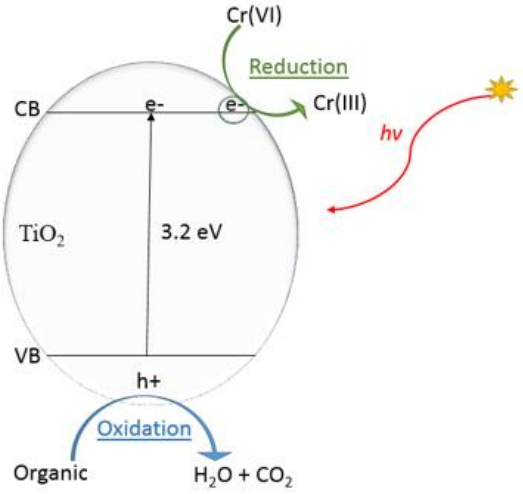

Figure 6. Schematic diagram of Cr(VI) reduction using TiO_2 photocatalytic process

TiO_2 doped with WO_3 has been investigated for photocatalytic reduction of Cr(VI) in the presence of citric acid as an electron donor.[44] Doping WO_3 onto TiO_2 can extend the absorption spectrum in the visible light region. This is because WO_3 has smaller band gap which allows the electrons to be trapped from TiO_2 to the WO_3 conduction band. As a result, photocatalytic reduction of Cr(VI) increased 3.76 times when the WO_3-doped TiO_2 was applied compared to using non doped TiO_2 .[45] Also, WO_3 can be doped onto

TiO_2 and be utilized as an electron storing material to be used during night time as discussed in section 2.1.2.

3 METHODOLOGY

3.1 Chemicals and reagents

Cr(VI) stock solution (1000 ppm) was prepared using $Na_2Cr_2O_7$ (Sigma Aldrich) in deionized water. Cr(VI) standards were prepared prior to each experiment to formulate the calibration carve for accurate Cr(VI) measurement.

WO_3 particles used in the experiments were obtained from Sigma-Aldeich and have particle size <100 nm. Two types of TiO_2 were used: Commercial TiO_2 nanoparticles P25(Sigma-Aldeich, anatase 80%, rutile 20%, 21 nm particle size) and synthesized TiO_2 nanotubes. TiNT were synthesized using microwave-assisted hydrothermal method.[46] Briefly, commercial TiO_2 powder was mixed in 10 N NaOH solution until homogenous suspension was observed. The solution was then treated at 1600 W for 1 hour using MARS microwave (MARSXpressTM vessel, CEM). The solution was then allowed to cool down and it was then vacuum filtrated. The nanotubes were washed by distilled water during vacuum filtration to wash out NaOH.

For all the experiments, the pH was adjusted using NaOH (Fisher Scientific) and HCl (VWR).

3.2 Analytical procedures

The concentration of Cr(VI) in the solution was measured following the standard method guided by the EPA.[47] Briefly, 10 mL of the sample was taken and allowed to react with 1 mL of dicarbazide solution in acidic media (0.250 mL of 2 M H_3PO_4 acid and 0.125 mL of concentrated H_2SO_4 acid) in order to form pink-colored complex. Also, each

standard solution was prepared by following the same way that is made for the samples. The concentration of Cr(VI) was quantified by UV-Visible Spectrometer (PerkinElmer, UV/VIS/NIR spectrometer, Lambda 950) at wavelength of 540 nm. The DL of Cr(VI) using this method range from 0.0044 to 0.015 µg/L.

Time profiles of the photocurrent were collected by a potentiostat (Camry Instrument) in a standard three-electrode system at constant potential of -0.4V vs. saturated calomel electrode (SCE). A Pt wire, a graphite rod and a saturated calomel electrode (SCE) were used as a working electrode, a counter and a reference electrode, respectively. Each TiO_2 sample (nanoparticle and nanotube) was suspended in 0.95 M NaOH solution with methyl viologen (MV^{2+}, 0.5 mM) as an electron mediator. N_2 gas was continuously purged for 1 hr of prior to irradiation and during irradiation.

The surface properties of TiNP or TiNT composites were characterized by surface analysis techniques, including X-ray photoelectron spectroscopy (XPS), photoluminescence spectroscopy (PL), X-ray diffraction (XRD), and scanning electron microscopy (SEM), in order to investigate surface crystallization, surface morphology, and surface-bound oxygen defect that can determine the behavior of charge carriers transfer at interface between solid and solution.

3.3 Materials preparation and experimental setup

3.3.1 Batch photocatalytic system

For batch photocatalytic system, commercial TiO_2 nanoparticles (TiNP) and synthesized TiO_2 nanotube (TiNT) were used for all batch experiments. Initial

concentrations Cr(VI) in these experiments was 2 mg/L and 2.5 mM formic acid was added as a hole scavenger. Sunlight irradiation of one sun (AM 1.5 and 100 mW/cm^2) was supplied using solar simulator (150-W Xenon Arc Lamp, ABET Tec.). The dose of TiNP or TiNT was varied in the range of 0.1 - 1 g/L to evaluate the effect of photocatalyst dose on the kinetics of Cr(VI) reduction at different pH values (pH3, 7, and 10).

3.3.2 Photoelectrochemical (PEC) system

3.3.2.1 Electrode preparation

For the PEC system, three different TiO_2/WO_3 composite materials were deposited on Fluorine doped Tin Oxide (FTO) glass with different weight ratios of TiO_2/WO_3 (TWx): TW 25, TW 50, and TW 75, where x represents the weight percentage of TiO_2 against WO3. For example, TW 25 indicates 25% TiO_2 and 75% WO_3 by wright.

Different weight ratios of TiO_2 and WO_3 were mixed with a pestle using 0.5 g/L polyethylene glycol (PEG) in ethanol and water mixture of 1:5 volume ratio. The mixture was then casted onto FTO glass (1cm x 2 cm) using 3 M adhesive tapes (0.048 mm thick) as spacers to make constant thickness of TiO_2/WO_3 photoelectrode. Finally, the electrodes were dried and annealed at 540 ^oC for 30 minutes to burn out the PEG.[18]

3.3.2.2 Photoelectrochemical test

In the PEC system, the fabricated TiO_2/WO_3 photoelectrode and graphite electrode were applied as working electrode and counter electrode, respectively (Figure 7), in the presence of aqueous electrolyte of 0.1 M Na_2SO_4. The TiO_2/WO_3 photoelectrode was first

charged by light irradiation from the solar simulator for one hour in the presence of 10 % ethanol by volume and 0.1M Na_2SO_4. Then the charged photoelectrode was used for reduction of Cr(VI) in water under light-limited condition in batch reactor of glass beaker. Water samples were taken at regular time intervals and analyzed for Cr(VI). In certain experiments, Cr(VI) was spiked in the water at the beginning of photoelectrode charging time to evaluate its reduction kinetics in the PEC system under light irradiation vs. its reduction in the dark during the discharging process. The extent of electron charging and discharging was monitored over time by the open circuit potential.

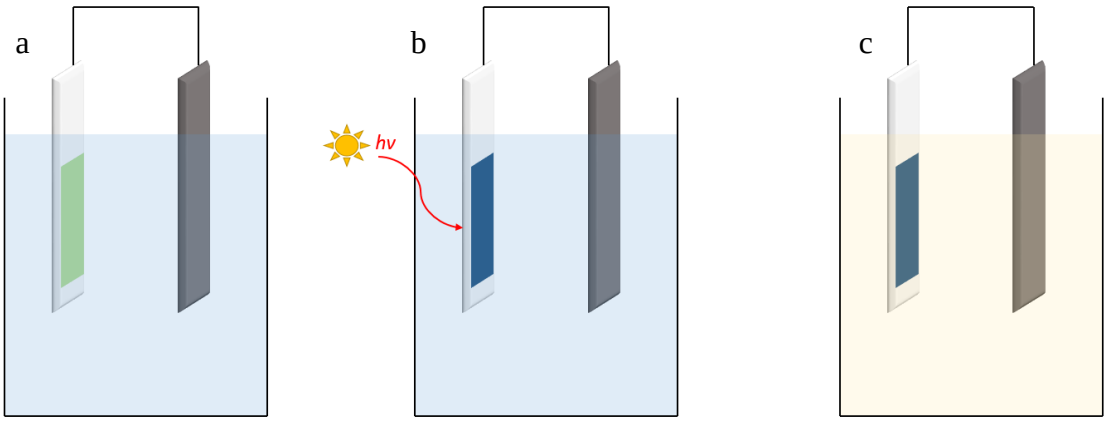

Figure 7. Experimental setup for charging of TiO_2/WO_3 heterojunction photoelectrode system a) before charging, b) while charging, and c) after charging

3.3.3 Membrane filtration system

3.3.3.1 Membrane preparation

TiO_2/WO_3-laden membrane filtration was developed and used for reduction of Cr(VI) in continuous flow system in the dark after charging the membrane under solar irradiation. To do so, first solutions of 0.25 g TiO_2 and 0.25 g WO_3 were added to 500 mL of water contacting 20% ethanol by volume. The solution was mixed together under sonication so that the final solution contains equal weights of TiO_2 and WO_3 (TW 50). Then 75 mL of the solution containing the solid was filtered through membrane filter (Anodisc, 20 nm pore diameter) using vacuum filtration allowing the TiO_2 and WO_3 solids to be deposited on the membrane surface as shown in Figure 8. In the course of charging the membrane under irradiation of solar light, ethanol drops were intermittently added on the membrane surface, which served as an electron donor in order to quickly and sufficiently charge the TiO_2/WO_3-deposited membrane under light irradiation. During the charging process, the color of the membrane changed from green to blue indicating that the TW50-laden membrane was charged. The same procedure was followed for case of 50 TiNT-W (50% TiNT by weight).

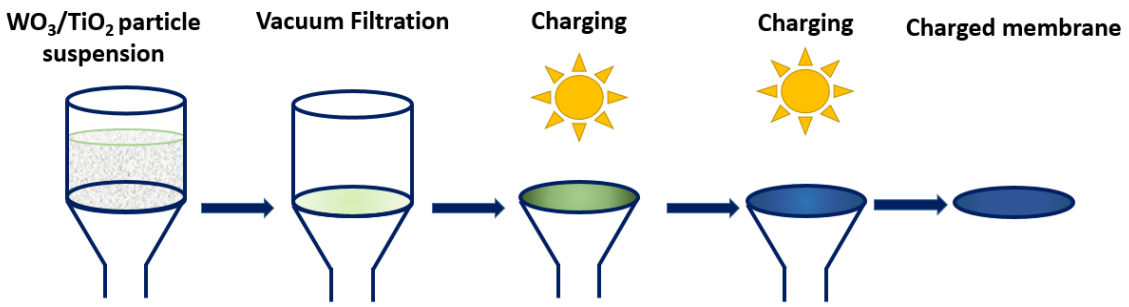

Figure 8. Photomembrane preparation

3.3.3.2 Experimental setup

For Cr(VI) reduction using the membrane filtration system, two different flow modes were applied: non-retentate mode and retentate (recycle) mode as shown in Figure 9 and Figure 10). In the case of non-retentate mode setup, the permeate water was collected over filtration time at fixed flowrate of 0.54 ml/min. For the retentate mode, a solution containing 200 ml of 0.125 ppm Cr(VI) solution was recycled with a fixed flow rate of 0.54 ml/min thought the membrane. In both cases, the solution was purged by N_2 during the experiment to obtain anoxic environment. Samples were collected at specified sampling times from water reservoir and analyzed for Cr(VI) concentration. The surface properties of charged and uncharged membranes were characterized using XPS and SEM before and after their use for Cr(VI) reduction experiments.

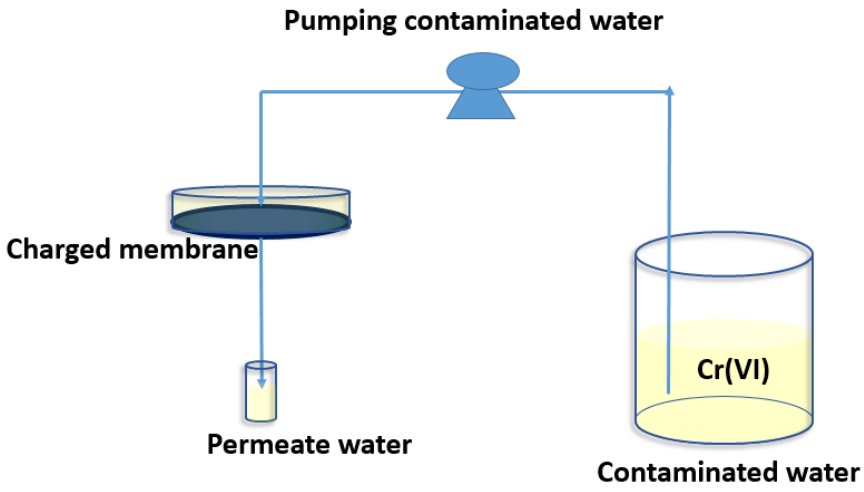

Figure 9. Experimental Set up for permeate water collection

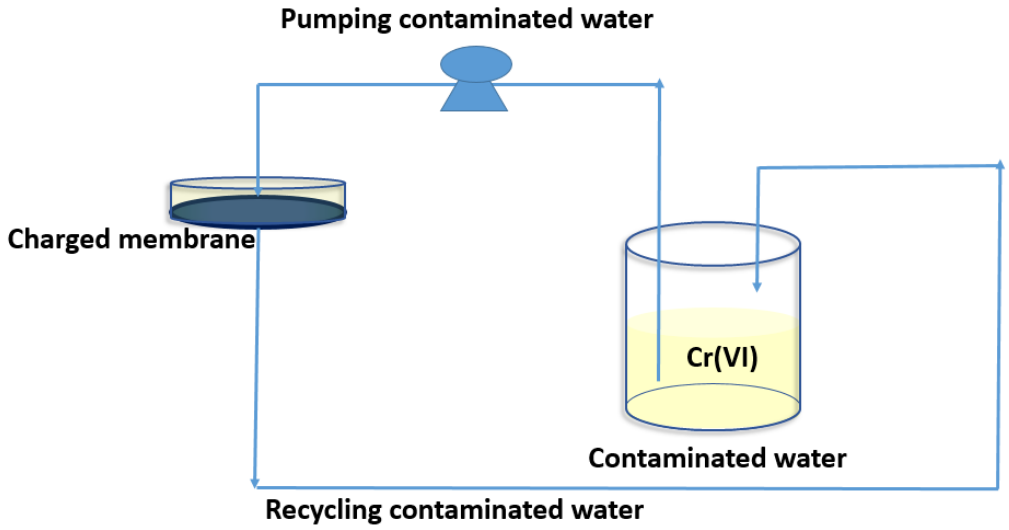

Figure 10. Experimental set up for recycling Cr(VI) using TW photomembrane

4 RESULTS AND DISCUSSION

4.1 Photocatalytic reduction of Cr(VI) using TiNP and TiNT composites

4.1.1 Surface characteristics of titanium dioxide particles

Figure 11 shows XRD patterns of nanostructured titanium dioxide samples, commercial TiO_2 nanoparticles (TiNP) and synthesized TiO_2 nanotubes (TiNT). All diffraction peaks were assigned to anatase (A) and rutile (R) phases by comparing the peaks with data from the literature.[48] The peak positions of anatase and rutile phases on TiNT and TiNP patterns showed that high temperature and high pressure did not affect significantly the formation of the TiO_2 precursor. Whereas the aspect ratio of the anatase and rutile for TiNP were 80% and 20%, respectively, and for TiNT were 41% and 35%, respectively, indicating the formation of a titanate structure (24%). It can be observed from the XRD patterns that nanotubes are less crystalline than nanoparticles.[49] The XRD peak of TiNT had a relatively broader with lower intensities than that of TiNP, indicating that the TiNT fabricated by hydrothermal method under strong base solution formed amorphous solids while TiO_2 nanoparticles that was treated by annealing with high temperature (> 400 ^{o}C) showed crystalline structure.[49]

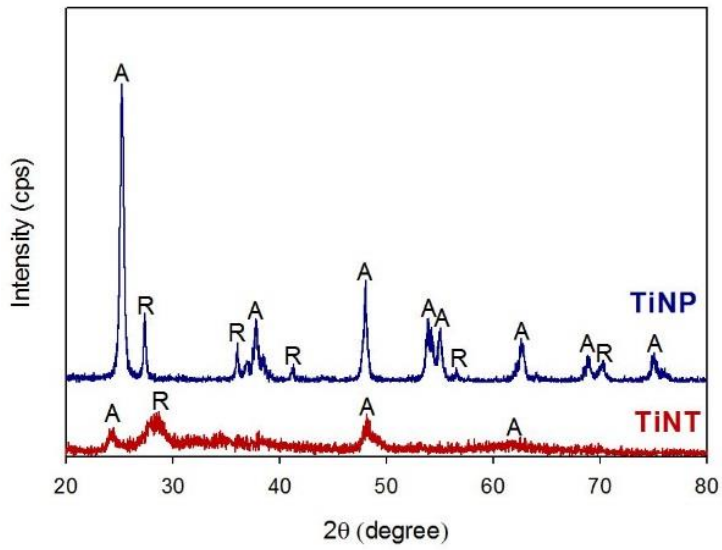

Figure 11. XRD patters for commercial TiO_2 nanoparticles (TiNP) and synthesized TiO_2 nanotubes (TiNT): anatase and rutile TiO_2 are labelled with A and B, respectively.

The morphological structures and particle sizes of TiNP and TiNT were further analyzed by TEM and SEM images (Figure 12). As shown by TEM images in Figure 12, TiNP and TiNT show granular solid with ~20 nm and wire-like structures with less than ~10 nm of diameter, respectively, confirming that TiO2 nanoparticles treated hydrothermally were transformed into the nanotubes. The SEM images show the snowflake-like assembly of nanoparticles and fiber-like cluster of nanotubes.

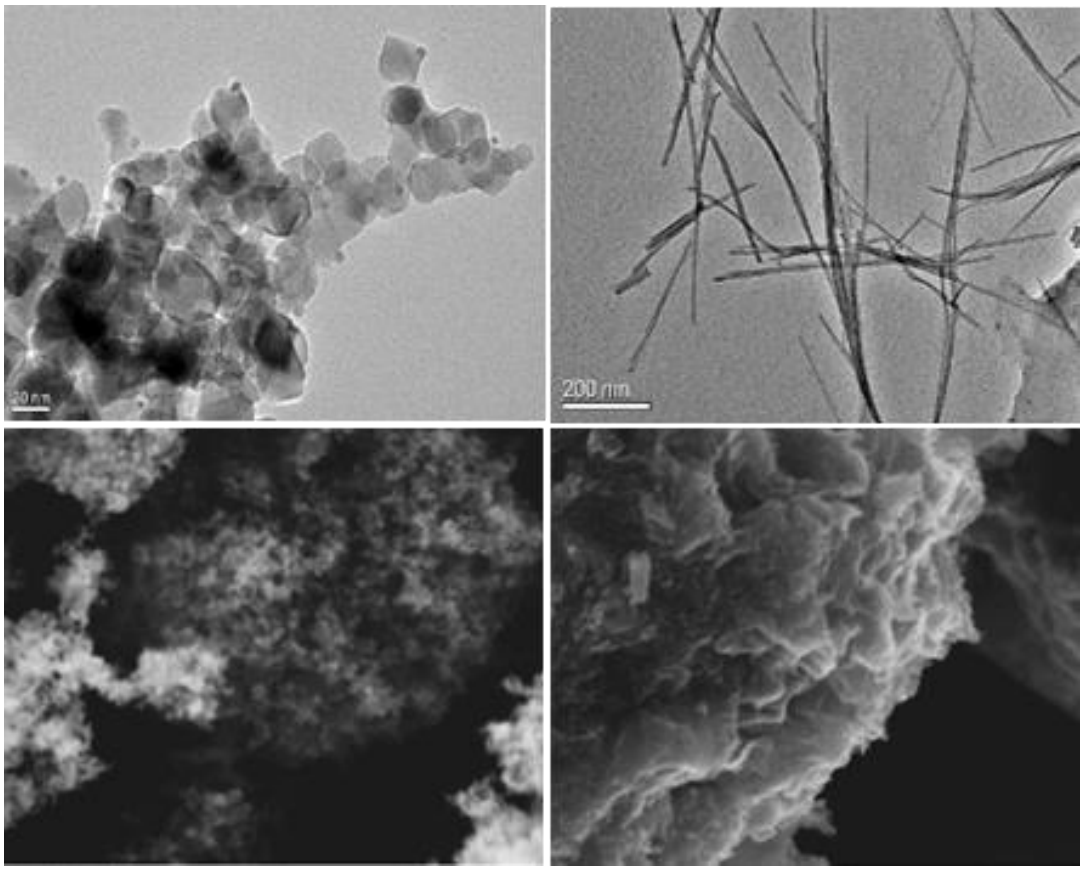

Figure 12. TEM images of (a) TiNP and (b) synthesized TiNT and SEM images of (c) TiNP and (d) TiNT.

The elemental composition of the surface of TiNP and TiNT solids were characterized by XPS, in which the atomic ratios of Ti and O were determined on the basis of the peak area from Ti 2p and O 1s XPS spectra in the survey spectra. The ratios of O/Ti were obtained with 2.4 for TiNT (O 1s/Ti 2p = 53.9: 22.4) and 0.4 for TiNP (O 1s/Ti 2p = 18.7: 50.8), respectively, indicating that TiNT sample has abundant oxygen whereas TiNP has oxygen defects. The O 1s spectra of TiNT and TiNP were deconvoluted to investigate oxygen species on the surface of each TiO_2 solid and the results are presented in Figure 13. Sub-bands of O 1s spectra at 529.4 eV, 529.8 eV and 530.3 eV were designated as O_I, O_{II} and O_{III} states, corresponding to lattice oxygens (Ti-O), chemisorbed oxygens (Ti-OH) and physically adsorbed oxygen (Ti-H_2O), respectively.[12,50] In the O 1s spectra of each TiO_2 sample, the fractions of the lattice oxygen (O_I) and the sorbed oxygens (O_{II} and O_{III}) were estimated to be 27.5% and 72.5% for TiNP, respectively, and 22.1% and 77.9% for TiNT, respectively. Compared to TiNP, TiNT has broader peak area of the Ti-OH and less in the Ti-O, indicating more structural oxygen defect in tubular TiO_2.

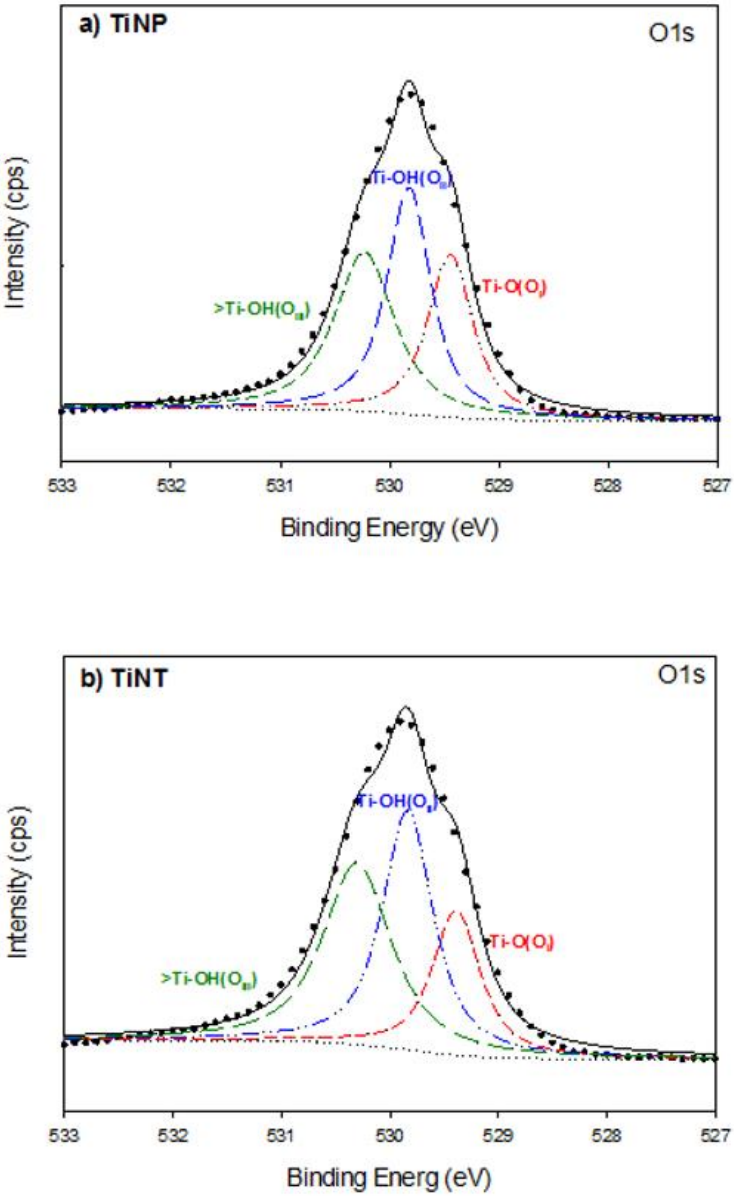

Figure 13. High resolution of O 1s XPS spectra for (a) TiNP and (b) TiNT

Figure 14 shows the Ti 2p XPS spectra where Ti $2p_{3/2}$ and Ti $2p_{1/2}$ peaks were located at 458.6 eV and 464.4 eV for TiNP, and at 458.3 eV and 464 eV for TiNT, respectively. In the Ti 2p spectra, Ti $2p_{3/2}$ and Ti $2p_{1/2}$ peaks represent Ti^{4+} ions and the region between the two peaks contribute Ti^{3+} ions that is mostly affected by the extent of structural oxygen defects.[12, 50, 51] Peak shift from TiNP to TiNT at lower binding energy value is attributed to the reduction of Ti^{4+} to Ti^{3+} ions on the surface of TiO_2.

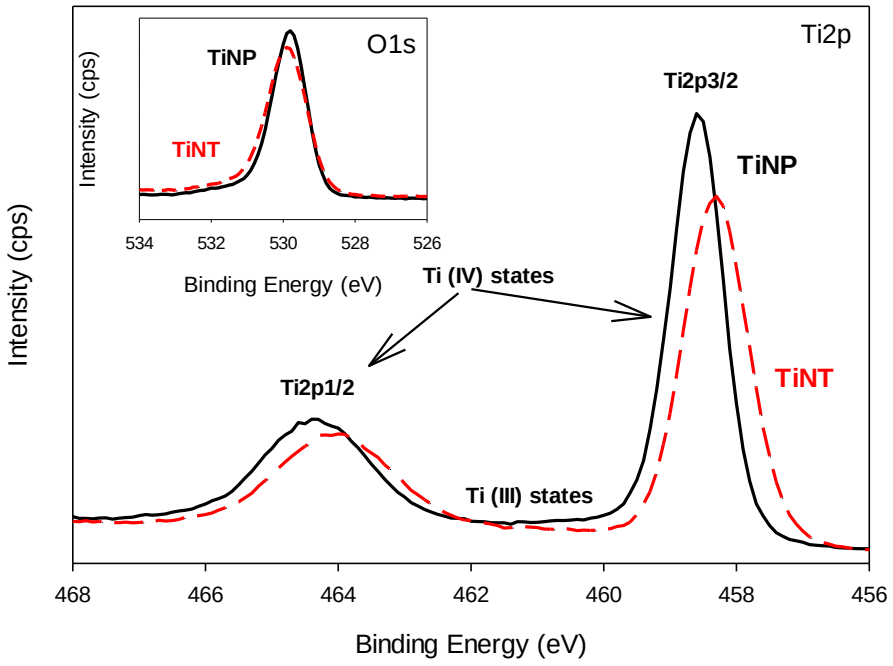

Figure 14. High resolution of Ti 2p XPS spectra for TiNP and TiNT samples

Photoluminescence (PL) spectra play a crucial role to determine the effectiveness of heterogeneous photocatalysis by investigating recombination states of photogenerated charge carriers and structural oxygen states.[52,53] In Figure 15, TiNP samples exhibit a

smaller wavelength emission bands (430-690 nm) than the bands (430-748 nm) of TiNT samples, designating that TiNP samples has less defect emission upon UV light emission. In other words, narrow width of the emission band can limit fast recombination of photogenerated charge carriers, which can result in more effective photocatalytic reaction on the surface of TiNP.[52]

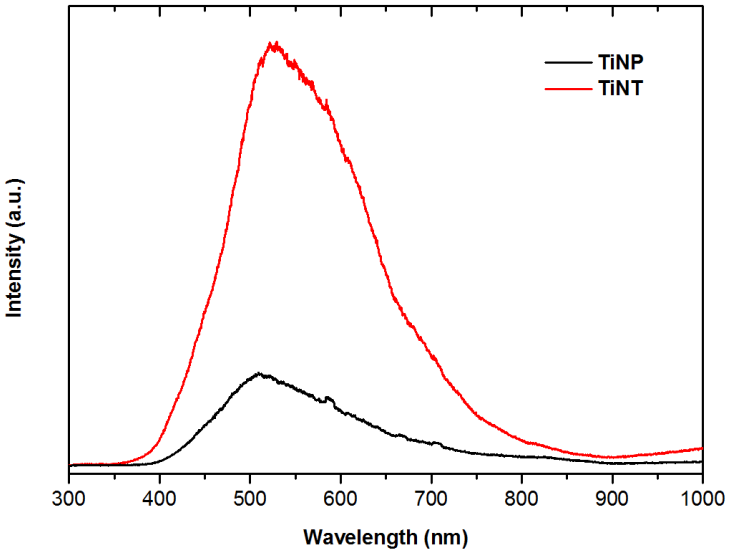

Figure 15. Photoluminescence spectra of TiNP and TiNP solid samples

Figure 16 shows the sub-bands of PL spectra of TiNP and TiNT samples that were fitted by Gaussian model. The peak position of 430 nm is attributed to be self-trapped excitons and blue-green emission bands (470 nm-550 nm) are often related to singly oxygen vacancies ($V_o^{\bullet}$) and neutral oxygen vacancies (V_o^{x}) below the conduction band edge. Red emission bands (630-690 nm) and yellow-red emission bands (590-748 nm) are attributed to surface states, which traps Ti atoms adjacent to interstitial oxygen (O_i)

localized at the surface area of TiO_2 structures. Compared to the level of oxygen states, TiNP and TiNT have 60.7% and 41.3% in oxygen vacancies, respectively and 38.3% and 55.9% in interstitial oxygen, respectively. Accordingly, TiNP samples have higher level of oxygen vacancies while TiNT samples reach to more prominent interstitial oxygen state. This is in agreement with XPS results shown in Figure 13.

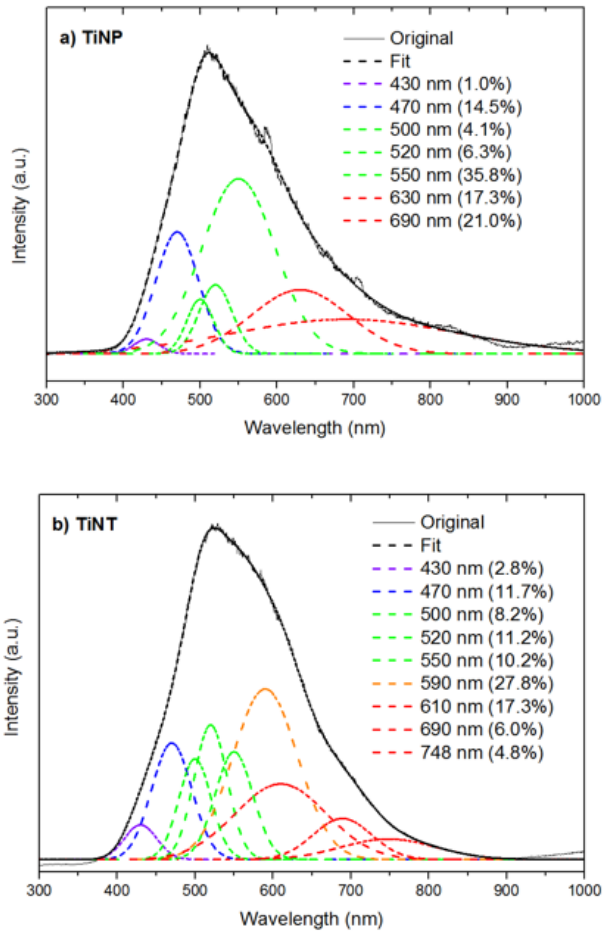

Figure 16. Room temperature photoluminescence (PL) spectra of two types of TiO2 in the range of UV: a) TiNP and b) TiNT. PL sub-bands fitted by Gaussian model have relative fractions to the range of UV emissions

Figure 18 shows photocurrent of TiNP and TiNT samples that was collected in a solid suspension under illumination of solar light (AM 1.5, 100 mW/cm^2). Through reaction (4.1-4.3), methyl viologen (MV^{2+}) played a role of electron shuttle by transferring photoelectron produced from conduction band of TiO_2 to Pt collector while the MV itself undergoes chemical reduction across the Pt/MV^+ interface (reaction 4.2 and 4.3).[54] The electron transfer are schematically represented in Figure 17.

$$TiO_2 + h\nu \rightarrow h + e^- \quad (4.1)$$

$$MV^{2+} + e^- \rightarrow MV^+ \quad (4.2)$$

$$MV^+ \rightarrow MV^{2+} + e^-_{(Pt)} \quad (4.3)$$

As a result, TiNP exhibited much higher photocurrent than TiNT by a factor of 11, attributed to the improved single-electron transfer efficiency.[49] As soon as the light is turned off, the rate of the photocurrent decay of TiNT was very rapid as compared to TiNP which shows relatively gradual decrease of the current until 8500 seconds, indicating slower recombination of charge carriers on the surface of TiNP.[55]

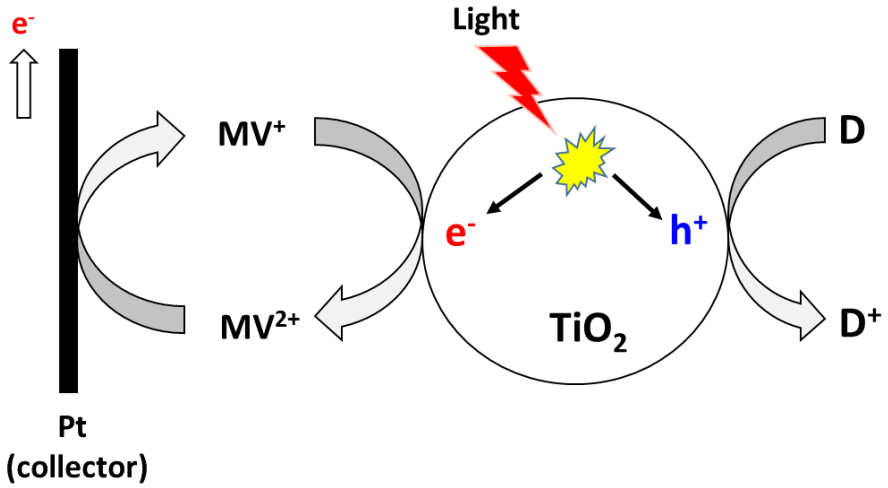

Figure 17. Schematic illustration of MV2+-mediated photocurrent measurement for irradiated TiNP and TiNT solids. D refers electron donor

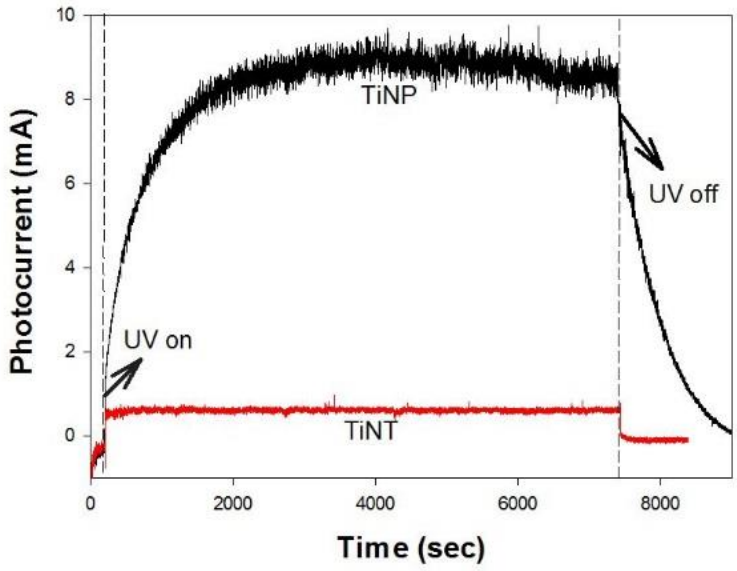

Figure 18. Photocurrent-time profiles of TiNP and TiNT at -0.4V vs. SCE under 1 sun of 1.5G solar illumination

.

The surface analyses of TiNP and TiNP using XPS, XRD, TEM and SEM indicated that the TiNP has abundant oxygen vacancies that is close to conduction band (CB) energy level, whereas TiNT have more oxygen interstitials close to valence band (VB) energy level as described by Figure 19.

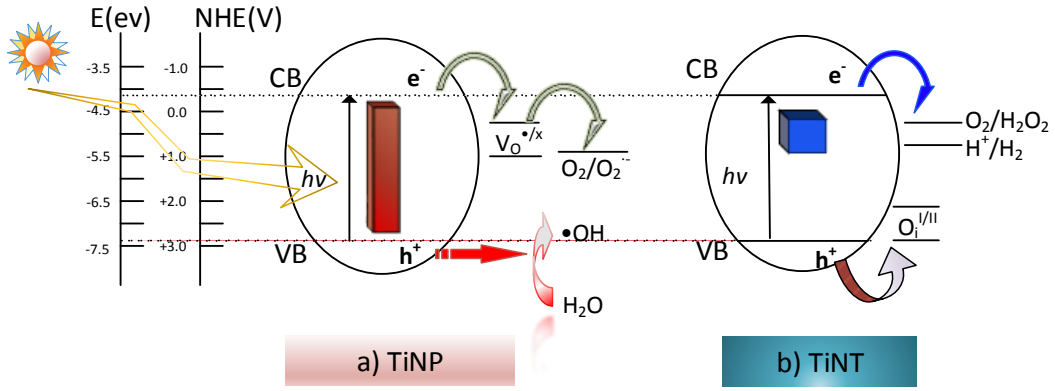

Figure 19. Schematic illustration of the photogenerated charge transfer events in the nanoparticles (TiNP) and nanotubes (TiNP) under light irradiation.

4.1.2 Kinetics of Cr(VI) reduction using TiNP and TiNT

To investigate the photocatalytic activities of TiNP and TiNT, Cr(VI) was chosen as a model target compound. A set of kinetic experiments for photoreduction of Cr(VI) were conducted at different pH values because it was reported in the literature that Cr(VI) reduction depends on the solution pH.[12] Figure 20 shows that Cr(VI) reduction with TiNP was faster than with TiNT, likely caused by more active single-electron transfer of TiNP for reducing Cr^{6+} to Cr^{3+}. Even though there are several steps required to reduce Cr(VI) to Cr(III) through single-electron transfer of irradiated TiO_2 suspension, Cr^{6+} can be rapidly

reduced to Cr^{3+} due to highly unstable intermediate Cr species of Cr^{5+} and Cr^{4+}. However, the rate and extent of Cr(VI) decay decreased with increasing of pH value regardless of the solid type and this observation was more substantial with TiNP than TiNT. At acidic pH, $HCrO_4^-$ is the dominant Cr(VI) and due to its negative charge, they are attracted to the positively charged surface of TiO_2 at range of pH<pHzpc (~6.0-6.5). Thus, high molecular density of $HCrO_4^-$ on the surface of TiO_2 at low pH enhances the electrochemical reaction between the photogenerated electrons on CB of TiO_2 and $HCrO_4^-$ that is sorbed on the surface of TiO_2. In contrast, the reduction rate of Cr(VI) decreased with increase of pH and was almost negligible for TiNT at both pH 7 and 10. These low reduction of Cr(VI) at > pH 7 might be attributed to formation of $Cr(OH)_3$ that can precipitate on the TiO_2 surface and deactivate the surface of the solids once photoreduction of Cr(VI) takes place.[56] In addition, less adsorption of Cr(VI) onto the surface of TiO_2 by electrostatic repulsion between negatively charged Cr(VI) and negatively charged TiO_2 at pH>pHzpc (~6.0) cannot be neglect for such slow reduction of Cr(VI).

The photocatalytic reduction of Cr(VI) was fitted to the Langmuir-Hinshelwood (LH) kinetics model (Eq.4.1) and as shown, the rate constants obtained by fitting the experimental results with LH model are presented in Table 4:

$$r = -\frac{d[\mathrm{Cr(VI)}]}{dt} = k_{LHR}\frac{k_{ad}C}{1+k_{ad}C} \qquad \text{(Eq.4.1)}$$

where k_{LHR}, k_{ad}, C, and t stand for LH rate constant, adsorption equilibrium constant, concentration of Cr(VI), and irradiation time, respectively.

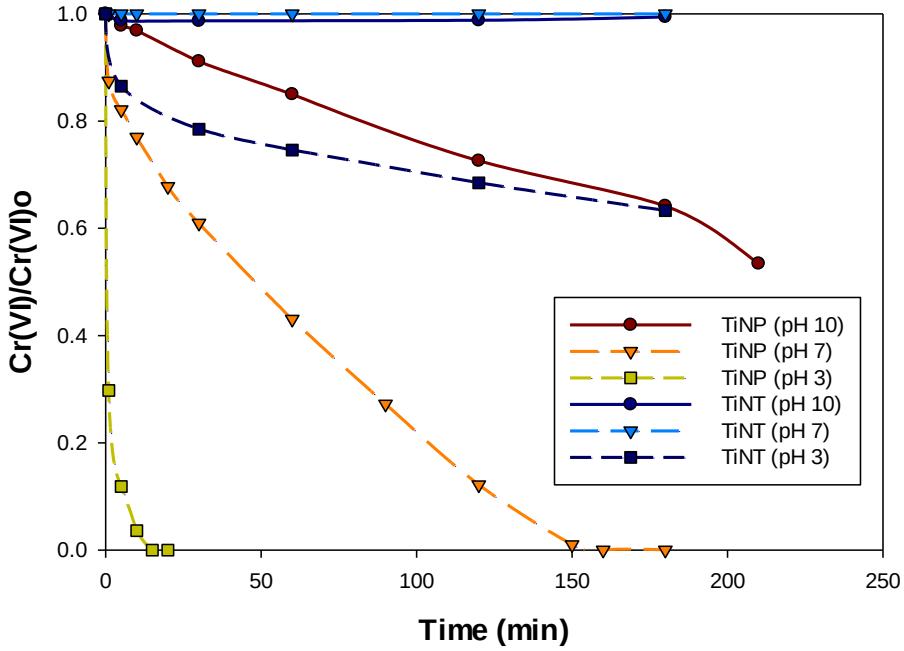

Figure 20. Kinetics of Cr(VI) reduction with TiNP and TiNT. Experimental conditions: 1 g/L solid and 2 ppm Cr(VI)

Table 4. Langmuir-Hinshelwood (LH) constants of Cr(VI) reduction using TiNP and TiNT

	TiNP			TiNT		
	pH 3	pH 7	pH 10	pH 3	pH 7	pH 10
k_{LHR} ($\mu mol \cdot L^{-1} min^{-1}$)	186.1362	4.7084	0.0105	6.9051	-	0.1354
k_{ad} ($\mu mol \cdot L^{-1}$)	0.0064	0.0037	0.33	0.0005	-	0.0009

4.2 Photoelectrocataytic (PEC) system using TiO_2/WO_3 heterojunction electrode

4.2.1 Open circuit potential (OCP)

The open circuit potential gives information about the potential of the working electrode relative to the reference electrode when no external potential is applied to the cell. Several parameters can affect the potential of TW-based PEC system, including the type of electrolyte, presence of electron donor, the coating area, the weight ratio of TiO_2 and WO_3, particle size and shape of the applied solids, and the charging time.[18]

Figure 21 shows the results of OCP for the TWx that was synthesized with different weight ratios of TiO_2 and WO_3, in which x refers to the x weight % of TiO_2 balanced with WO_3. For the case of composite material of TiNT and WO_3, 25% TiO_2 was balanced with 75 % WO_3 by weight (i.e., TNW 25). As shown in Figure 21, the magnitude of the charged potential during charging time decreased to more negative value as TiO_2 content increased. This indicates that influential factor for determining the magnitude of the electron charging in the TiO_2-WO_3 composite is directly related to large portion of TiO_2 against WO_3 (i.e., TW 75). Even though the TW 75 has more negative potential, the rate of releasing the electrons during discharging time was observed to be fast in the same TW 75. This might be caused by less amount of electrons captured by relatively less portion of WO_3 in the TiO_2-WO_3 composite through neutralization with proton, which quickly diminished once it was contacted with solution containing electron scavengers (e.g., O_2). Accordingly, TW 25 showed relatively long lag time in releasing the electrons to the solution, while TNW 25 showed faster release of electrons than TW 25. TNW 25 also has lower magnitude of OCP than TW 25. This is due to less crystallinity of TiO_2

especially anatase-type TiO_2 after treating them hydrothermally at high concentration of NaOH to make nanotube structure, eventually resulting in poor photocatalytic activity of TiNT. This hypothesis can be proven by XRD data in Figure 11, showing more broaden and lower intensity of the XRD peak for TiNT than TiNP.

Such a OCP display pattern during and after charging TW with respect to loading ratio of TiO_2 and WO_3 are in a good agreement with results reported by Park et al.[18] For example, the charging period for TW material was slow and at least one hour was required to drop the potential from -0.37 V to – 0.46 V for TW 75.

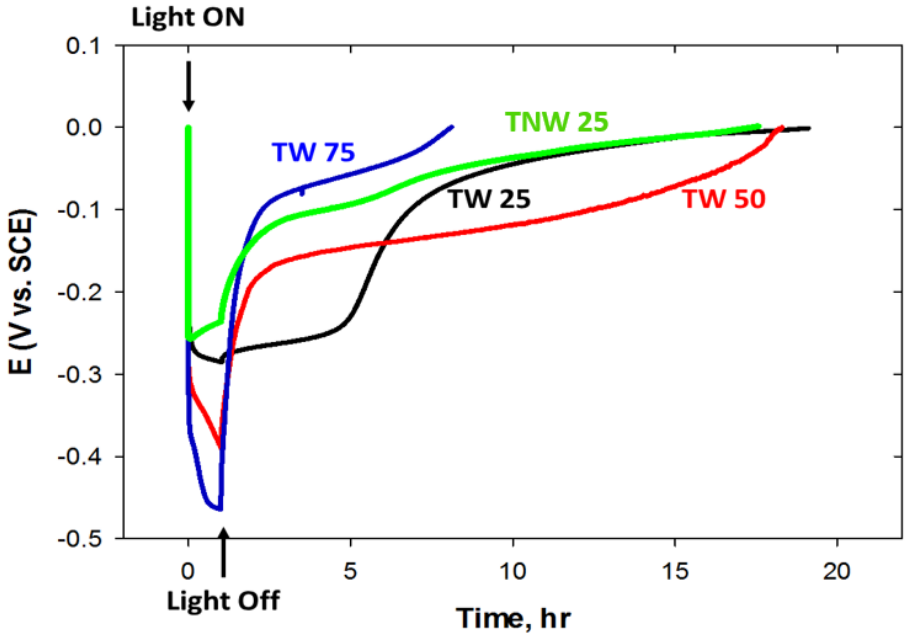

Figure 21. Effects of TW weight ratios on the changes of (OSP) and discharging times. Electrolyte 0.1 M Na_2SO_4

4.2.1 Surface analysis of photoelectrodes

4.2.1.1 SEM and elemental mapping

SEM images and elemental mapping of the TW electrode materials (i.e., TW 25, TW 50, TW 75, and TNW 25) were analyzed to investigate the status of particle distribution of each solid (TiO_2 or WO_3), elemental composition and quantity after deposition and annealing. Regardless of type of materials, two distinct separation of particle assembly were seen in the SEM images where large size and rock-like particles are deposited on the background-like layer composed of very fine and thick particles assembly (Figure 22). According to the elemental mapping data, TiO_2 particles is a major component in the bottom layer supporting WO_3 particles above this layer. These particles position can lead to more effective transfer of the photogenerated charge carriers from TiO_2 to WO_3 (Figure 23).

Based on the particle sizes of TiO_2 (~10 nm) and WO_3 (~1 μm), the small TiO_2 particles act as a support layer by making a film that uphold larger WO_3 particles which tend to aggregate and form a rock-like particles. However, larger-sized aggregates of TNW were formed as compared to TW particles, due to longer tubular shape of TiO_2 with high surface area that allow many accessible sites which facilitate aggregation.

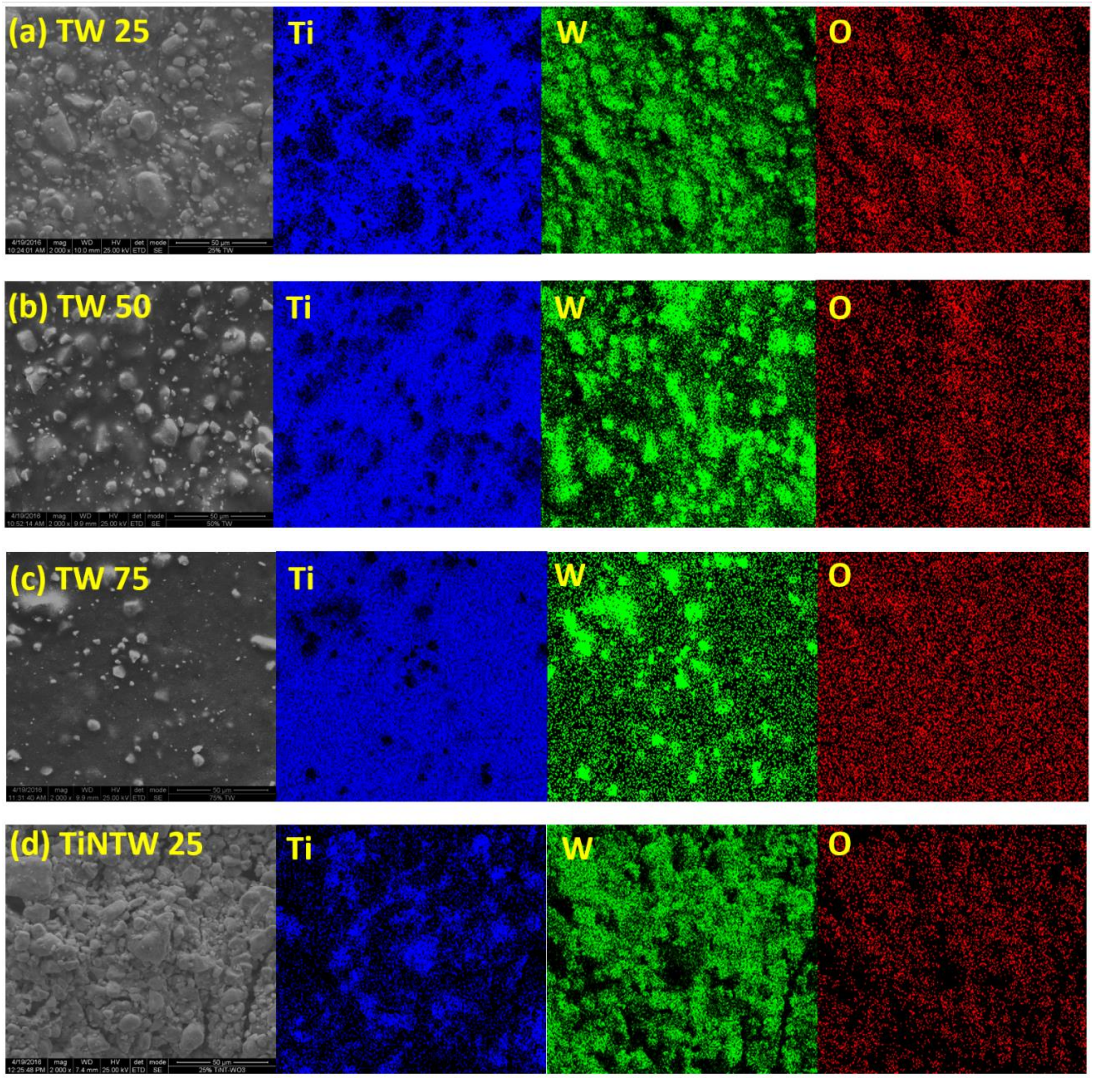

Figure 22: SEM images and elemental mapping of mixed TW electrodes a) TW 25, b) TW 50, c) TW75, and d) TiNTW 25

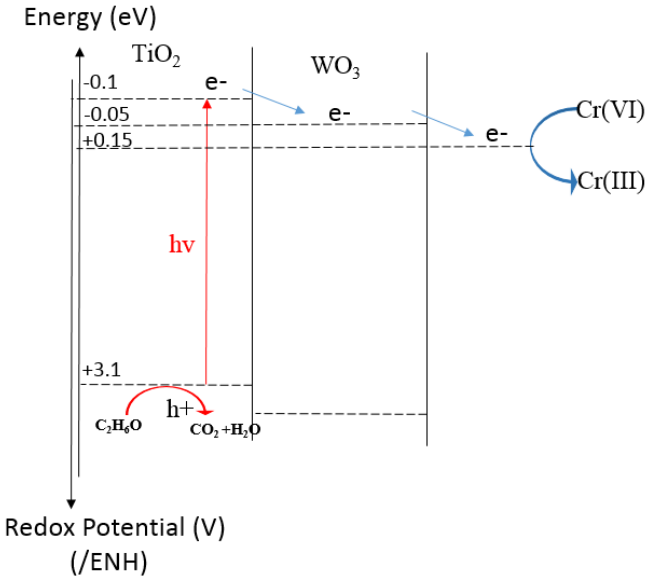

Figure 23. Schematic diagram for the transfer of charge carriers between TiO_2 and WO_3

4.2.1.2 EDS

Figure 24 represents the EDS data for TW and TNW electrodes (TW 25, TW 50, TW 75, and TNW 25). According to the elemental composition data shown in Figure 24 and by excluding % portion of oxygen from the total percentage of elements, ratios of Ti to W in TW 25, TW 50, TW 75, and TNW 25 are calculated to be 24 %, 44.4 %, 62 %, and 24 %, respectively. TW 75 material shows 17 % deviation from theoretical ratio of 75 % for Ti/W. This could be caused by covering the bottom layer TiO_2 particles under the largely aggregated WO_3 particles formed above the TiO_2 layer, presumably leading to somewhat more identification of WO_3 than TiO_2. However, it can be concluded that mixtures of TiO_2 and WO_3 to obtain the desired ratio for each TW material was successfully prepared.

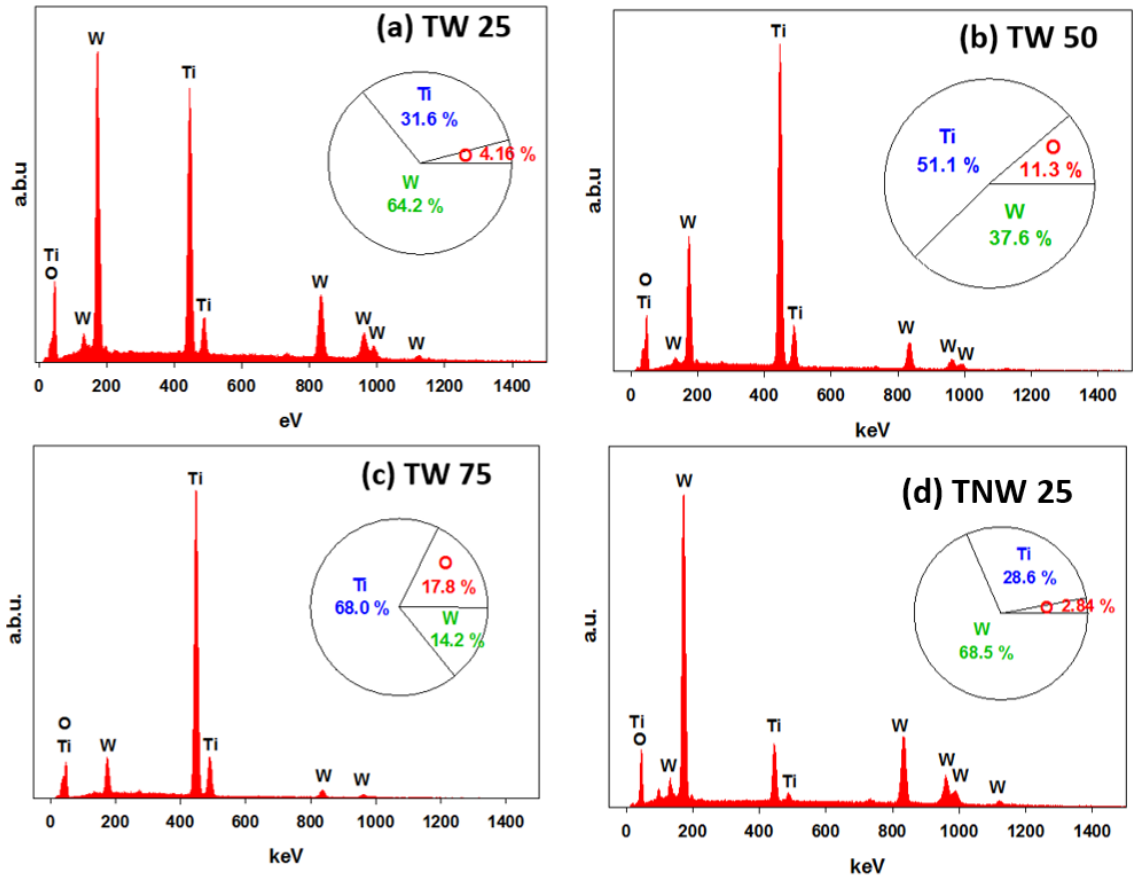

Figure 24. EDS mixed TW electrodes a) TW 25, b) TW 50, c) TW75, and d) TNW 25

4.2.1.3 V light absorbance of TW photoelectrodes

Figure 25 presents the UV-Vis spectra of TW photoelectrodes with different solid weight ratios as well as TNW 25. The obtained reflectance spectra were converted to absorption values using the Kubelka-Munk equation.[57] Regardless of weight ratios of TiO_2/WO_3 and type of TiO_2, the four materials showed similar trend for absorption spectra. Furthermore, two apex points of the absorption spectra took place approximately at ~310 and ~375 nm, which resulted from the mixture of two photocatalysts with different

band-edge position. At the wavelength range of 370-400 nm, the absorption spectra of TW materials are distinctly separated, in which the extent of absorption spectra increases as the content of WO_3 increases. This is due to higher photoactivity of WO_3 by lower band gap energy of 2.8 eV than TiO_2 (3.8 eV). Moreover, the absorption spectra of TNW 25 is greater that TW 25. This results contradicts data reported in the literature which showed that TiO_2 nanotube has larger band gab energy (3.6 eV) than TiO_2 nanoparticles (2.8 eV).[58] This contradiction might be due to the uneven particles distribution on the FTO glass. The extrapolation of the slope for the four photoelectrode materials give wavelength around 320 nm, which corresponds to a band gap energy of 3.8 eV. The resulted band gap is larger than the band gap of the individual homogenous materials TiO_2 (3.2 eV) and WO_3 (2.8).

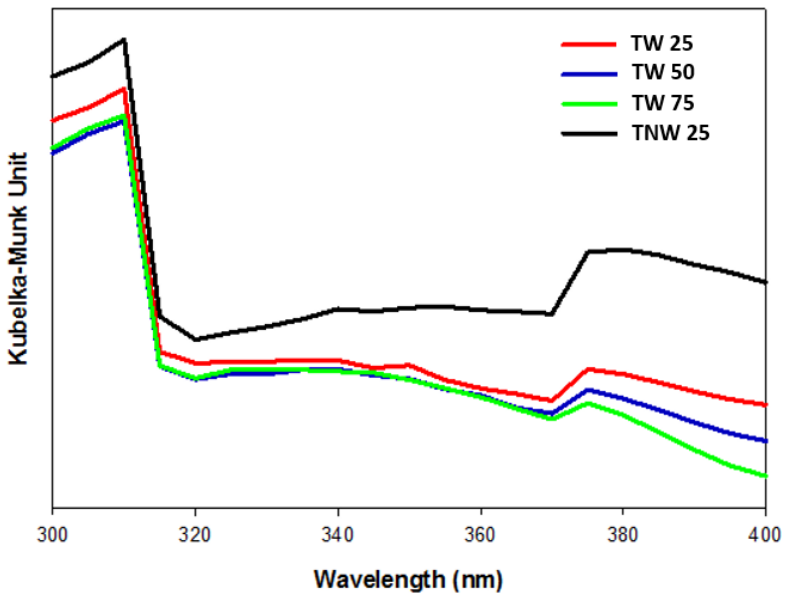

Figure 25. UV-Vis spectra of TW material with different solid weight ratios and of TNW 25

4.2.2 Cr(VI) reduction with TiO_2/WO_3 photoelectrodes

Prior to investigating photocatalytic reduction of Cr(VI) by TW photoelectrode, the photoelectrode was charged for 1 hour under solar light irradiation. Then the charged electrode was used in a batch reactor system for Cr(VI) reduction in the dark. Figure 26 shows that complete removal of Cr(VI) was observed with TW 25 and TW 50 in 3 hours. The rate of Cr(VI) reduction increased with increasing the WO_3 weight ratio due to increasing electron storing capacity as the ratio of WO_3 in the photoelectrode material increased. However, TNW 25 achieved faster Cr(VI) reduction rate than TW25 at initial discharging time even though both have the same weight ratio of TiO_2/WO_3. Based on OCP data in Figure 21, TNW 25 has a lower OCP value than TW 25 during the charging time and also the rate of electron release during discharging time was faster for TNW 25 than TW 25. Thus, this may induce TNW 25 to have faster Cr(VI) reduction at initial time but slow reduction over longer discharging time.

As TW 25 electrode presents the best performance for Cr(VI) reduction, it was used in subsequent experiments for further characterization of Cr(VI) reduction in the PEC system. Figure 27 shows the effect of initial Cr(VI) concentration on its reduction rate and indicates that TW 25 was able to completely reduce Cr(VI) in 4.5 hours for all initial concentrations that were investigated, but with increasing the reduction rate as initial Cr(VI) concentration decreased.

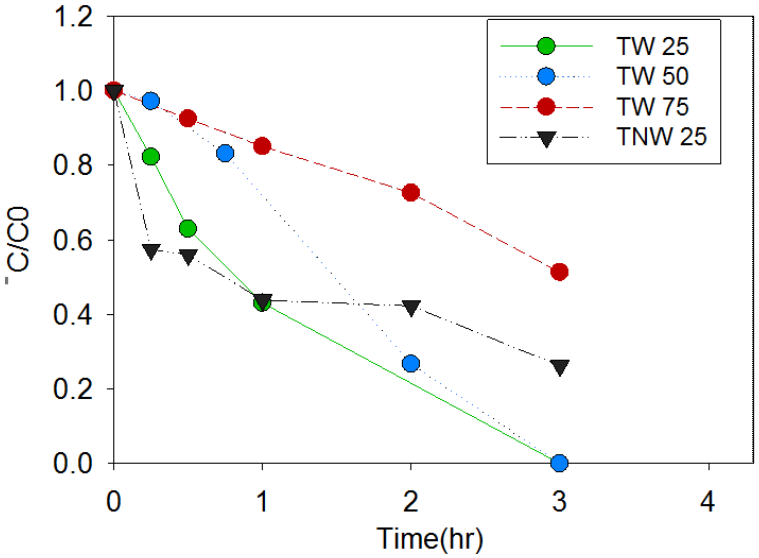

Figure 26. Cr(VI) removal in photoelectrode system using $Co_{Cr(VI)}$ =0.25 ppm

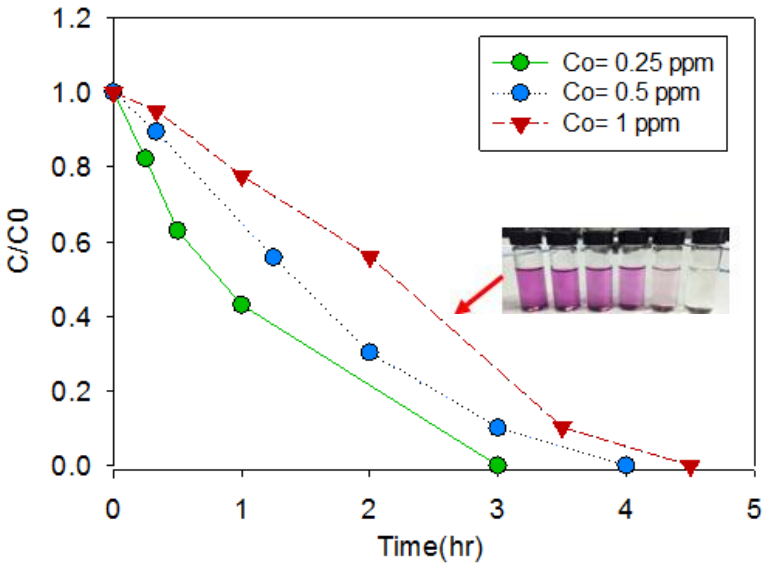

Figure 27. Cr(VI) removal in photoelectrode system using TW 25

Previous experiments investigated Cr(VI) reduction with TW electrodes in the dark during night time. However, it is important to evaluate its reduction in the same system during daytime and the extent of charging TW25 electrode during Cr(VI) reduction process under solar irradiation. Figure 8 shows the kinetics of Cr(VI) reduction TW electrode under solar irradiation during the TW charging period of 1 hour and the extent of its continuous reduction after the light is turned off. During the charging time, TW 25 can remove 55 % of 0.25 ppm initial Cr(VI) concentration and the removal continued during the discharging time after the light was turned off until complete removal was obtained in 4 hrs of the entire contact time. This implies that TW 25 electrode was still being charged during Cr(VI) reduction under solar irradiation and the charged TW 25 continued to remove Cr(VI) in the absence of light. Similar Cr(VI) removal pattern was observed in the case where Cr(VI) was spiked only after charging time. This indicates that the TW photoelectrode has the ability to reduce Cr(VI) during both daytime and night time.

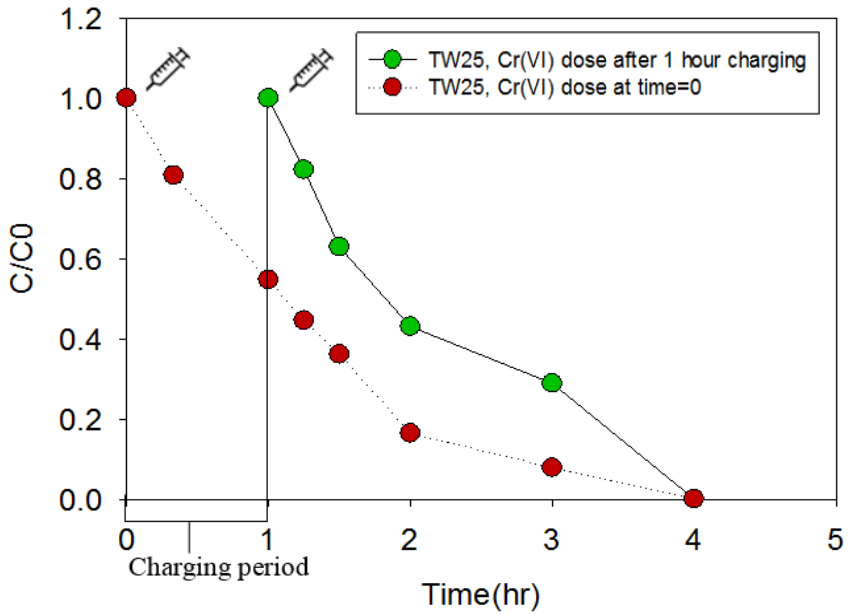

Figure 28. Cr(VI) reduction using TW 25 during charging and discharging, initial Cr(VI) concentration = 0.25 ppm

4.3 Cr(VI) reduction using photocatalytic membrane system

TW-deposited membrane system was developed and evaluated for Cr(VI) reduction. TW 50 and TNW 50 were deposited on the membrane filter discs and then charged by solar light irradiation and the charged membranes were used for Cr(VI) reduction in continuous flow system in the absence of light.

4.3.1 SEM/EDS analysis and elemental mapping of TW membranes

The surface of the charged TW50-laden membranes were characterized using SEM/EDS and elemental mapping analysis technique to investigate the surface morphology and % of elemental composition on the membrane surface. As shown in Figure 29, co-existence of large particles assembly and very fine particles assembly were observed on the TW-laden membrane surface. Based on elemental mapping, the large particles assembly are mostly composed of WO_3 whereas TiO_2 particles contributed to a regular distribution of small particles without any considerable formation of clusters. Also, the EDS analysis shows elemental ratio of 59 % Ti : 45 % W. If we consider portion of the % Oxygen element in each particle, TW would be composed of near 50:50 of elemental ratio, eventually proving successful deposition of TW materials (50:50 %) onto the filtration membrane disc.

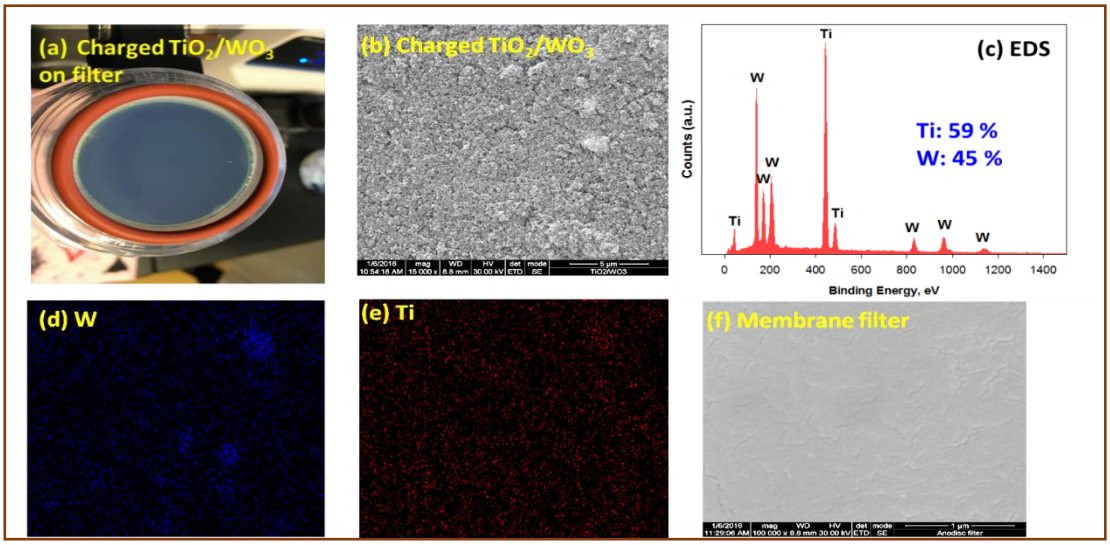

Figure 29. SEM/EDS analysis and elemental mapping of charged TiO_2/WO_3 membrane

4.3.2 Cr(VI) reduction using TW-laden membrane system

Two filtration modes were applied for Cr(VI) reduction: 1) Dead-end filtration mode, and 2) Retentate filtration mode. Figure 9 represents a dead-end filtration mode with 0.54 mL/min of flowrate where permeate water samples was collected over filtration time and the concentrations of Cr(VI) in permeate water were measured in the collect samples. For the control test of Cr(VI) reduction, an uncharged TW 50 membrane was applied to investigate the extent of Cr(VI) removal by adsorption onto the membrane material. Figure 30 shows that Cr(VI) concentration in the permeate water from the uncharged membrane filter was quickly resumed back to its initial concentration as compared to the cases with charged membranes and remained at the maximum level of C/C0=1, indicating that the membrane is not active in reducing Cr(VI) or adsorbing Cr(VI). In the case of charged TW 50 membrane, the system shows a better Cr(VI) reduction when the system was purged with nitrogen rather than the case when the system was not purged with nitrogen. For example, in the N_2-purged TW 50 membrane system Cr(VI) concentration in the permeate water was ~70 % of the initial concentration in 4 hours as compered to 92% in the non-N_2 purged system. Herein, the remaining 30% reduction of initial Cr(VI) concentration indicates that the TW 50-deposited filtration membrane has a capacity to reduce Cr(VI) and the reduction coulsd be enhanced if more contact time is allowed. This is evident by observing the color change of the charged TW 50-deposited filtration membrane before and after filtration of Cr(VI) solution, showing co-presence of light blue color (during charging) and green color (before charging) as shown in Figure 32.

In order to allow more contact time of Cr(VI) with the TW50 deposited on the membrane surface, a filtration experiment was carried out with a retentate filtration mode. In this experiment, the filtered water was continuously recycled. And Cr(VI) concentration in the permeate was measured over time. Unlike the dead-end filtration mode, the retentate filtration mode shows continuous removal of Cr(VI) over filtration time by gradualy converting Cr(VI) to Cr(III) through continuous contact of Cr(VI) with TW 50 or TNW 50. TW 50 material was extremely more effective in Cr(VI) removal than TNW 50 as shown in Figure 31. This is also evident color of the the TW 50 and TNW 50 deposited on the membrane surface, showing more thick blue color in the TW 50 than in the TNW 50. This could be caused by the charge transfer from the WO_3 in TNW 50 to Cr(VI) occurring very quickly and consumed all the capacity in 1 hour of filtration time. Similar result and pattern of TNW material regarding Cr(VI) removal was observed in the photoelectrode system, exhibiting quick consumption of the charged electrons at initial contact time (Figure 26)

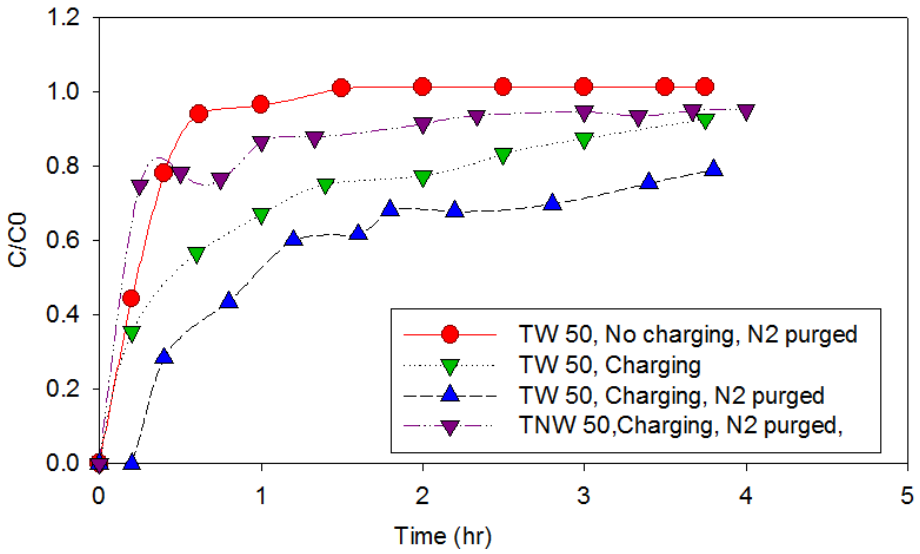

Figure 30. Cr(VI) concentration in permeate water. Flow=0.54 ml/min and $C0_{Cr(VI)}$ =0.25 ppm

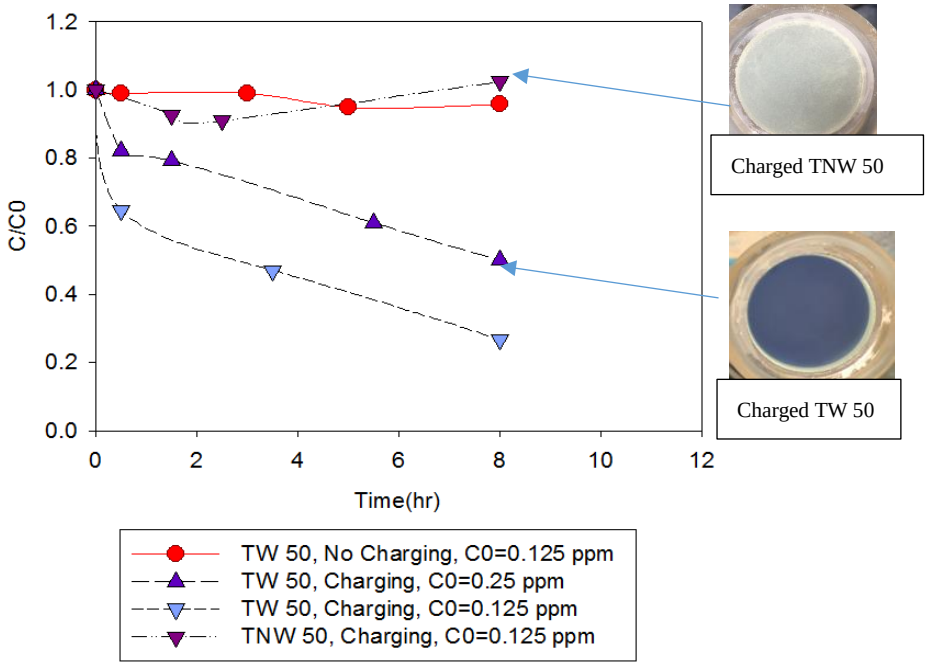

Figure 31. Cr(VI) reduction using N_2 purged system. Flow=0.54 ml/min

4.3.3 XPS analysis

In order to better understand whether the Cr(VI) removal mechanism in the photocatalytic membrane system is due adsorption chemical reduction, the membrane surface was characterized using XPS analysis. Figure 34 did not show a high signal-to-noise Cr2p XPS spectra, indicating that there is no significant amount of chromium adsorbed on the membrane surface and that Cr(VI) was immediately reduced to Cr(III) by electron transfer from the charged TW and the unreduced Cr(VI) passed through the filter with the permeate water (Figure 33). Accordingly, the W 3d XPS spectra were collected for samples of the charged and uncharged TW 50 material before and after treating Cr(VI) solution. In both cases, the uncharged TW 50 materials did not show no substantial change of W $4d_{5/2}$ peaks, indicating no oxidation change in the W element. However, the oxidation status of tungsten in the W $4d_{5/2}$ spectra was observed in the charged TW 50 materials, where the central peak of the W(III) assigned to 247.8 eV was shifted to lower range of the binding energy. This means that the WO_3 in TW 50 were photochemically reduced with a chemical structure of $H_xW^{(6-x)}O_3$, along with cghaning the color of the material to blue (see embedded image in Figure 35) . After treating Cr(VI) solution, the charged TW 50 material started chemical oxidation of W element, but it is not fully oxidized resulting in the co-existence of both structural $W^{(6-x)}$ and W^{6+} from $H_xW^{(6-x)}O_3$. The co-existence of the two oxidation states of the tungsten resulted in more broaden central point of the W$4d_{5/2}$ peak.

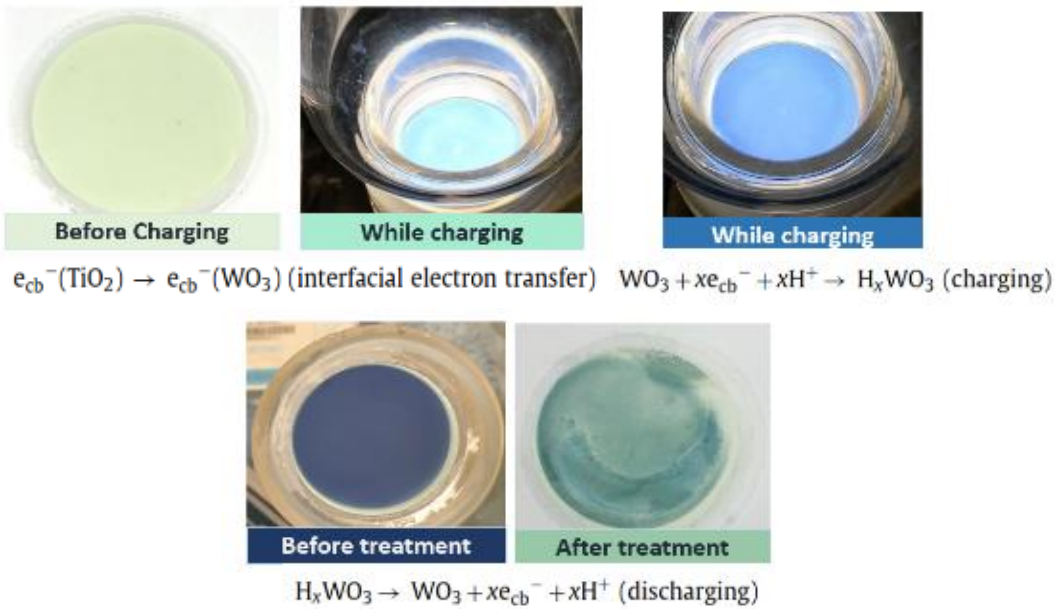

Figure 32. TW membrane before charging, while charging, before treatment, and after treatment.

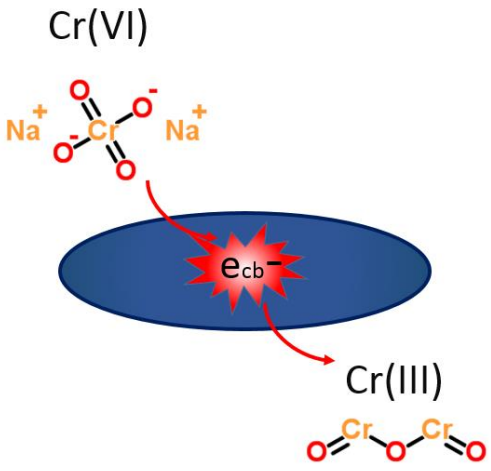

Figure 33. Cr(VI) reduction to Cr(III) in the membrane due to electron transfer

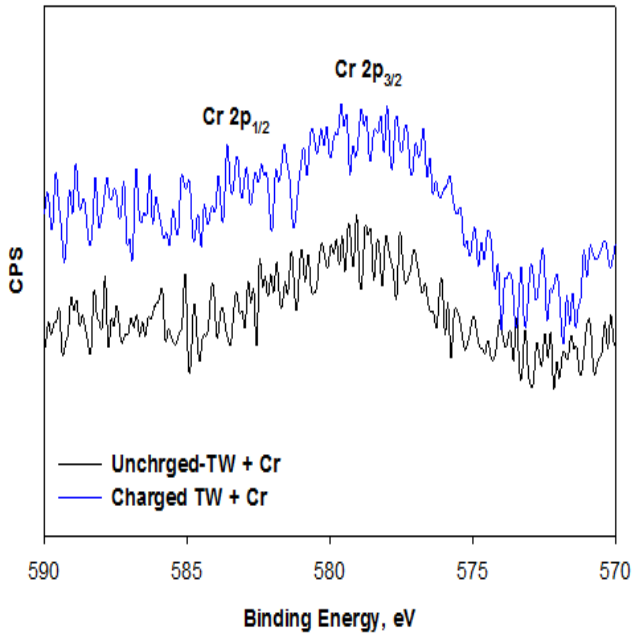

Figure 34. XPS analysis of Cr(VI) on the charged and uncharged membrane

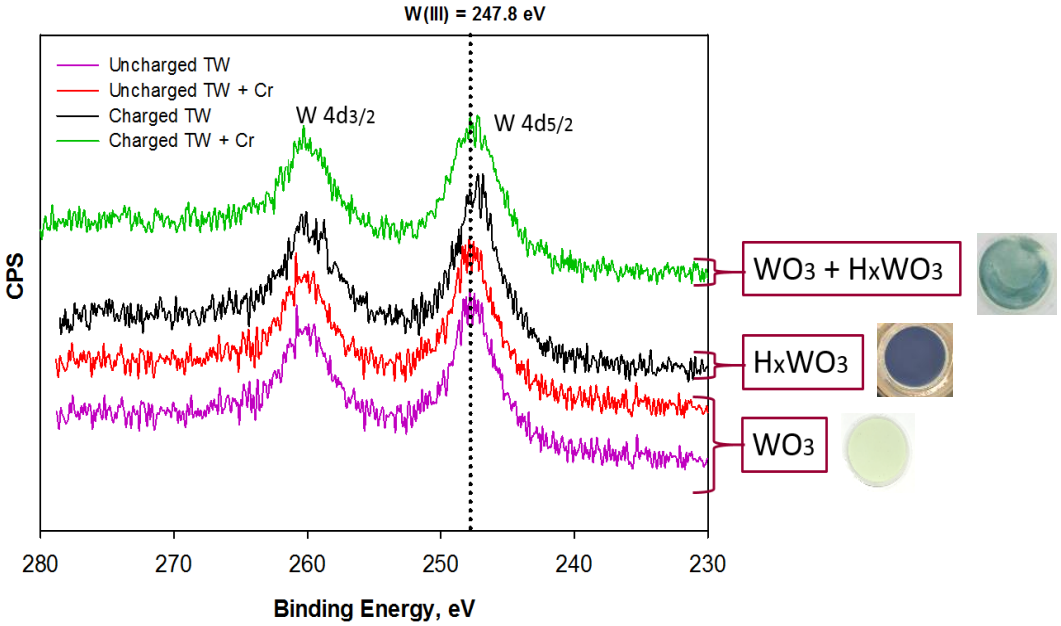

Figure 35. XPS analysis of W on TW membrane with 50% TiO_2 by weight

5 CONCLUSIONS

In this research, TiO_2-WO_3 composite materials were developed to store solar energy that was used to reduce Cr(VI) in water under light-limited condition. Meanwhile, different shapes of TiO_2 particles (granular type of TiO_2 nanoparticle (TiNP), tubular type of TiO_2 nanoparticle (TiNT)) were employed to investigate effect of surface morphology on catalytic activities and their capacities for conversion of Cr(VI) to Cr(III). A series of experiments for Cr(VI) removal was performed with three different systems: Batch catalytic system, Photoelectrochemical (PEC) system, and filtration membrane system.

The batch system using TiO_2 nanoparticles (TiNP) showed rapid and complete Cr(VI) removal at low pH and at neutral pH in 2.5 hours of solar light irradiation time (PM 1.5, 100 $mWcm^{-2}$). However, the batch system using TiNT were not as effective as the system using TiNP at low pH. The effect of surface morphology on photocatalytic activity was investigated by using surface analysis techniques, including PL, XPS, XRD, TEM, and SEM/EDS. The surface analysis can be summarized as the following:

- XRD data showed that TiNP are more crystalline that TiNT.
- XPS showed that TiNP have less structural oxygen defects.
- PL spectra and photocurrent time profile showed that TiNP have slower recombination of the photogenerated electrons than TiNT.
- PL sub-bands showed that TiNP have more oxygen vacancies closer to CB while TiNT have more interstitial oxygen close to VB.

The results of the batch system proved that TiNP has a greater photocatalytic activity than TiNT. The results of the batch system were used to design and describe the systems where TiNP and TiNT are combined with WO_3, for continuous removal of Cr(VI) in light limited conditions.

In the PEC system, TW 25, TW 50, TW 75, and TNW 25 electrodes have been synthesized and used to evaluate their catalytic ability on Cr(VI) reduction. Among these electrodes, TW 25 had the longest discharging time according to the OCP data and also showed the best performance in completely reducing Cr(VI) into Cr(III) in ~ 3 and 4.5 hours for initial Cr(VI) concentrations of 0.25 ppm and 1 ppm, respectively, under dark condition (discharging time). In addition, the TW 25 has the ability to remove Cr(VI) during charging time, ensuring a continuous treatment of Cr(VI) for the period of both diurnal and nocturnal time. However, TNW 25 (25% weight ratio of TiNT to WO_3) can remove 70 % of initial Cr(VI) concentration in 4 hours of reaction time at identical condition that was given to experiment using TW 25. Using TiO_2 nanoparticle-based TW 25 rather than TiO_2 nanotube-based TNW 25 would be an advantage of the PEC system as it ensures a continuous treatment of Cr(VI) during daytime and night time.

The photocatalytic membrane filtration system using TiO_2-WO_3 composite materials showed the feasibility of reducing Cr(VI) to Cr(III) when Cr(VI) solution contacts the materials deposited on the membrane surface by the electrons stored during the charging time. The Cr(VI) conversion was shown to be more effective with the TW materials rather than TNW material. This is consistently in agreement with the results of the PEC system. The XPS analysis of the membrane proved that Cr(VI) removal in the

membrane system was due to electron transfer between the Cr(VI) and TW material and that there is no significant amount of chromium absorbed onto the membrane surface. Also, the W 3d XPS spectra of the TW 50-deposited membrane after charging showed that the central peak of the W(III) assigned to 247.8 eV was shifted to lower range of the binding energy, meaning that the WO_3 in TW 50 are photochemically reduced with a chemical structure of $H_xW^{(6-x)}O_3$. After reducing Cr(VI), the center point of the W 3d peak in the TW 50 material became wider, indicating the existence of different oxidation states of W.

REFERENCES

1. Waughray, D.; Workman, J., National Security. In *Water security : the water-food energy-climate nexus : the World Economic Forum Water Initiative*. Washington, DC, 2011; pp 88-110.

2. Watkins, K., Human Development Report 2006 *Beyond scarcity: Power, poverty and the global water crisis.* United Nations Development Program. NY, 2006.

3. Herrmann, J. M., Heterogeneous Photocatalysis: Fundamentals and Applications to the Removal of Various Types of Aqueous Pollutants. *Catalysis Today* 1999, 53, 115-129

4. Zhang, F.; Itoh, H., Photocatalytic Oxidation and Removal of Arsenite from Water Using Slag-iron Oxide-TiO_2 Adsorbent. *Chemosphere* 2006, 65 (1), 125-131.

5. Liu, B. ; Zhao, X.; Terashima, C.; Fujishima, A.; Nakata, K., Thermodynamic and Kinetic Analysis of Heterogeneous Photocatalysis for Semiconductor Systems. *Phys. Chem. Chem. Phys* 2014, 16, 8751-8760.

6. Serp, P.; Machado, B., *Nanostructured Carbon Materials for Catalysis*. Cambridge : Royal Society of Chemistry, Cambridge: 2015.

7. Barakat, M. A., New Trends in Removing Heavy Metals from Industrial Wastewater. *Arabian Journal of Chemistry* 2011, *4*, 361-377.

8. Tiehu, H.; Dongmei, Z.; Huigang, W.; Xuming, Z., Preparation and Photocatalytic Activities of p-n Heterojunction Cu_2O/TiO_2 Nanoparticles. *Key Engineering Materials* 2016, *671*, 444-449.

9. Wang, M.; Sun, L.; Lin, Z.; Cai, J.; Xie, K.; Lin, C., p-n Heterojunction Photoelectrodes Composed of Cu_2O-loaded TiO_2 Nanotube Arrays with Enhanced Photoelectrochemical and Photoelectrocatalytic Activities. *Energy & Environmental Science* 2013, *6* (4), 1211-1220.

10. Dozzi, M. V.; Marzorati, S.; Longhi, M.; Coduri, M.; Artiglia, L.; Selli, E., Photocatalytic Activity of TiO_2-WO_3 Mixed Oxides in Relation to Electron Transfer Efficiency. *Applied Catalysis B: Environmental* 2016, *186*, 157-165.

11. Dey, T., Nanotechnology for Water Purification. *Nuclear Desalination* 2010, 4, 49-57.

12. Wu, Q.; Zhao, J.; Qin, G.; Wang, C.; Tong, X.; Xue, S., Photocatalytic Reduction of Cr(VI) with TiO_2 Film Under Visible Light. *Applied Catalysis B, Environmental* 2013, 142-148.

13. Tan, Y.; Beydoun, D.; Amal, R., Photocatalytic Reduction of Se(VI) in Aqueous Solutions in UV/TiO_2 System: Importance of Optimum Ratio of Reactants on TiO_2 Surface. *Journal of Molecular Catalysis A: Chemical* 2003, *202*, 73-85.

14. Skubal, L. R.; Meshkov, N. K., Reduction and Removal of Mercury from Water using Arginine-Modified TiO_2. *Journal of Photochemistry and Photobiology A: Chemistry* 2002, *148*, 211-214.

15. Litter, M. I., Treatment of Chromium, Mercury, Lead, Uranium, and Arsenic in Water by Heterogeneous Photocatalysis. In *Advances in Chemical EngineeringPhotocatalytic Technologies* 2009; 36, 37-67.

16. Smith, W.; Zhao, Y., Superior Photocatalytic Performance by Vertically Aligned Core–Shell TiO_2/WO_3 Nanorod Arrays. *Catalysis Communications* 2009, *10*, 1117-1121.

17. Kim, S.; Park, H., Sunlight-Harnessing and Storing Heterojunction $TiO_2/Al_2O_3/WO_3$ Electrodes for Night-Time Applications. *RSC Adv* 2013, 3, 17551-17558.

18. Park, H.; Bak, A.; Jeon, T. H.; Kim, S.; Choi, W., Photo-Chargeable and Dischargeable TiO_2 and WO_3 Heterojunction Electrodes. *Applied Catalysis B Environmental* 2012, 115, 74-80.

19. Ngaotrakanwiwat, P.; Tatsuma, T.; Saitoh, S.; Ohko, Y.; Fujishima, A., Charge–Discharge Behavior of TiO_2–WO_3 Photocatalysis Systems with Energy Storage Sbility. *Phys. Chem. Chem. Phys* 2003, 5, 3234-3237

20. *Chromium Toxicity: Case Studies in Environmental Medicine*. Agency for Toxic Susbstances and Disease Registry: Atlanta,GA, 2011, 1-67.

21. Shupack, S. I., The chemistry of chromium and some resulting analytical problems. *Environmental Health Perspectives* 1991, *92*, 7-11.

22. What are chromium's health effects? U.S. Environmental Protection Agency: Washington, DC. https://safewater.zendesk.com/hc/en-us/articles/212077277-03-What-are-chromium-s-health-effects (Accessed Aug 21, 2015).

23. *Toxic Substances Portal Chromium.* Agency for Toxic Susbstances and Disease Registry: Atlanta,GA http://www.atsdr.cdc.gov/substances/toxsubstance.asp?toxid=17 (Accessed Nov 19, 2015)

24. Wetterhahn, K. E.; Hamilton, J. W., The Chromium Paradox in Modern Life Molecular Basis of Hexavalent Chromium Carcinogenicity: Effect on Gene Expression. *Science of The Total Environment* 1989, *86* (1), 113-129.

25. Zhitkovich, A.; Voitkun, V.; Kluz, T.; Costa, M., Utilization of DNA-protein Cross-Links as a Biomarker of Chromium Exposure. *Environmental Health Perspectives* 1998, *106*, 969-974.

26. Table of Regulated Drinking Water Contaminants. U.S. Environmental Protection Agency: Washington, DC. https://www.epa.gov/ground-water-and-drinking-water/table-regulated-drinking-water-contaminants#Inorganic. (Accessed Jan 11, 2016)

27. Emsley, J., *The Elements.* Clarendon Press 1998.

28. Tong, Y.; Ke-An, L., The Distribution Of Chromium(V1) Species In Solution as a Function of pH and Concentration. *Talanta* 1986, *33*, 115-717.

29. Kimbrough, D. E.; Cohen, Y.; Winer, A. M.; Creelman, L.; Mabuni, C., A Critical Assessment of Chromium in the Environment A Critical Assessment of Chromium in the Environment. *Critical Reviews in Environmental Science and Technology* 1999, *291*, 1-461.

30. Barrera-Díaz, C. E.; Lugo-Lugo, V.; Bilyeu, B., A review of chemical, electrochemical and biological methods for aqueous Cr(VI) reduction. *Journal of Hazardous Materials* 2012, *223-224*, 1-12.

31. Jardine, P.; Fendorf, S.; Mayes, M.; Larsen, I.; Brooks, S.; Baily,W., Fate and Transport of Hexavalent Chromium in Undisturbed Heterogeneous Soil. *Environ. Sci. Technol* 1999, *33*, 2939-2944

32. Barrera-DíIaz, C.; Urena, F.; Campos, E.; Palomar-Pardav, M.; Romero-Romo, M., A Combined Electrochemical-Irradiation Treatment of Highly Colored and Polluted Industrial Wastewater. *Radiation Physics and Chemistry* 2003, *67*, 657-663.

33. Emamjomeh, M.; Sivakumar, M., Review of Pollutants Removed by Electrocoagulation And Electrocoagulation/Flotation Processes. *Journal of Environmental Management* 2009, *90*, 1663-1679.

34. Almaguer-Busso, G.; Velasco-Martínez, G.; Carreño-Aguilera, G.; Gutiérrez-Granados, S.; Torres-Reyes, E.; Alatorre-Ordaz, A., A comparative Study of

Global Hexavalent Chromium Removal by Chemical and Electrochemical Processes. *Electrochemistry Communications* 2009, *11*, 1097-1100.

35. Geo Enviro Solutions. Waste Water Treatment Plant. http://www.geoenvirosolution.in/waste-water-treatment-plant.html (Accessed Jul 5, 2015)

36. Ruotolo, L. A. M.; Santos-Júnior, D. S.; Gubulin, J. C., Electrochemical Treatment of Effluents Containing Cr(VI) Influence of pH and Current on the Kinetic. *Water Research* 2006, *40*, 1555-1560.

37. Mary Mangaiyarkarasi, M. S.; Vincent, S.; Janarthanan, S.; Subba Rao, T.; Tata, B. V. R., Bioreduction of Cr(VI) by Alkaliphilic Bacillus Subtilis and Interaction of the Membrane Groups. *Saudi Journal of Biological Sciences* 2011, *18*, 157-167.

38. Xu, L.; Luo, M.; Li, W.; Wei, X.; Xie, K.; Liu, L.; Jiang, C.; Liu, H., Reduction of Hexavalent Chromium by Pannonibacter Phragmitetus LSSE-09 Stimulated with External Electron Donors Under Alkaline Conditions. *Journal of Hazardous Materials* 2011, *185*, 1169-1176.

39. Fukuda, T.; Ishino, Y.; Ogawa, A.; Tsutsumi, K.; Morita, H., Cr(VI) Reduction from Contaminated Soils by Aspergillus sp. N2 and Penicillium sp. N3 Isolated from Chromium Deposits. *The Journal of General and Applied Microbiology* 2008, *54*, 295-303.

40. Rengaraj, S.; Li, X. Z., Enhanced Photocatalytic Reduction Reaction Over Bi^{3+}–TiO_2 Nanoparticles in Presence of Formic Acid as a Hole Scavenger. *Chemosphere* 2007, *66*, 930-938.

41. Tan, T.; Beydoun, D.; Amal, R., Effects of Organic Hole Scavengers on the Photocatalytic Reduction of Selenium Anions. *Journal of Photochemistry and Photobiology A: Chemistry* 2003, *159*, 273-280.

42. Reynal, A.; Lakadamyali, F.; Gross, M. A.; Reisner, E.; Durrant, J. R., Parameters Affecting Electron Transfer Dynamics from Semiconductors to Molecular Catalysts for the Photochemical Reduction of Protons. *Energy Environ. Sci.* 2013, *6*, 3291-3300.

43. Mu, R.; Xu, Z.; Li, L.; Shao, Y.; Wan, H.; Zheng, S., On the Photocatalytic Properties of Elongated TiO_2 Nanoparticles for Phenol Degradation and Cr(VI) Reduction. *Journal of hazardous materials* 2010, *176*, 495-502.

44. Yang, Q. L.; Kang, S. Z.; Chen, H.; Bu, W.; Mu, J., $La_2Ti_2O_7$: An Efficient and Stable Photocatalyst for the Photoreduction of Cr(VI) Ions in Water. *Desalination*, 2011; 266, 149-153.

45. Yang, L.; Xiao, Y.; Liu, S.; Li, Y.; Cai, Q.; Luo, S.; Zeng, G., Photocatalytic Reduction of Cr(VI) on WO_3 Doped long TiO_2 Nanotube Arrays in the Presence of Citric Acid. *Applied Catalysis B: Environmental* 2010, *94*, 142-149.

46. Rajabzadeh, G. H.; Firuzian, A.; Hamzelahzadeh, P., Microwave Assisted Synthesis of TiO_2 Nanotube : Influence of Irradiation Power , Temperature and

Pressure on its Photocatalytic Activity and Morphology . *Proceedings of the 4thInternational Conference on Nanostructures (ICNS4)* 2012, 12-14.

47. *A Compendium of Chemical, Physical and Biological Methods for Assessing and Monitoring the Remediation of Contaminated Sediment Sites*. U.S. Environmental Protection Agency, Office of Water Engineering and Analysis Division: Washington, DC. 2015

48. Qian, X.; Qin, D.; Song, Q.; Bai, Y.; Li, T.; Tang, X.; Wang, E.; Dong, S., Surface Photovoltage Spectra and Photoelectrochemical Properties of Semiconductor-Sensitized Nanostructured TiO_2 Electrodes. *Thin Solid Films* 2001, *385*, 152-161.

49. Jeong, H. W.; Choi, S. Y.; Park, H.; Hong, S. H.; Lim, S. K.; Han, D. S.; Abdel-Wahab, A., Shape-Dependent Charge Transfers in Crystalline ZnO Photocatalysts: Rods Versus Plates. *Journal of Physical Chemistry C* 2014, *118* (37), 21331-21338.

50. Yu, J.; Dai, G.; Huang, B., Fabrication and Characterization of Visible-Light-Driven Plasmonic Photocatalyst Ag/AgCl/TiO_2 Nanotube Arrays. *Journal of Physical Chemistry C* 2009, *113* (37), 16394-16401.

51. Ku, Y.; Jung, I.-L., Photocatalytic Reduction of Cr(VI) in Aqueous Solutions by UV irradiation with the presence of Titanium Dioxide. *Water Research* 2001, *35*, 135-142.

52. Testa, J. J.; Grela, M. A.; Litter, M. I., Heterogeneous Photocatalytic Reduction Of Chromium(VI) Over TiO_2 Particles in the Presence of Oxalate: Involvement Of Cr(V) Species. *Environ. Sci. Technol* 2004, 38 (5), 1589-1594.

53. Vinu, R.; Madras, G., Kinetics of Simultaneous Photocatalytic Degradation of Phenolic Compounds and Reduction of Metal Ions With Nano-TiO_2. *Environ. Sci. Technol* 2008, 42 (3), 913-919.

54. Qian, X.; Qin, D.; Song, Q.; Bai, Y.; Li, T.; Tang, X.; Wang, E.; Dong, S., Surface Photovoltage Spectra And Photoelectrochemical Properties of Semiconductor-Sensitized Nanostructured TiO_2 Electrodes. *Thin Solid Films* 2001, *385* (1), 152-161.

55. Yu, J. G.; Dai, G. P.; Huang, B. B., Fabrication and Characterization of Visible-Light-Driven Plasmonic Photocatalyst Ag/AgCl/TiO_2 Nanotube Arrays. *Journal of Physical Chemistry C* 2009, *113* (37), 16394-16401.

56. Wang, X. L.; Pehkonen, S. O.; Ray, A. K., Removal of Aqueous Cr(VI) by a Combination of Photocatalytic Reduction and Coprecipitation. *Industrial & Engineering Chemistry Research* 2004, *43* (7), 1665-1672.

57. *Diffuse Reflectance – Theory and Applications; PIKE Technologies* 2011.

58. Ou, H.-H.; Lo, S.-L., Review of Titania Nanotubes Synthesized Via the Hydrothermal Treatment: Fabrication, Modification, and Ppplication. *Separation and Purification Technology* 2007, 58 (1), 179-191.